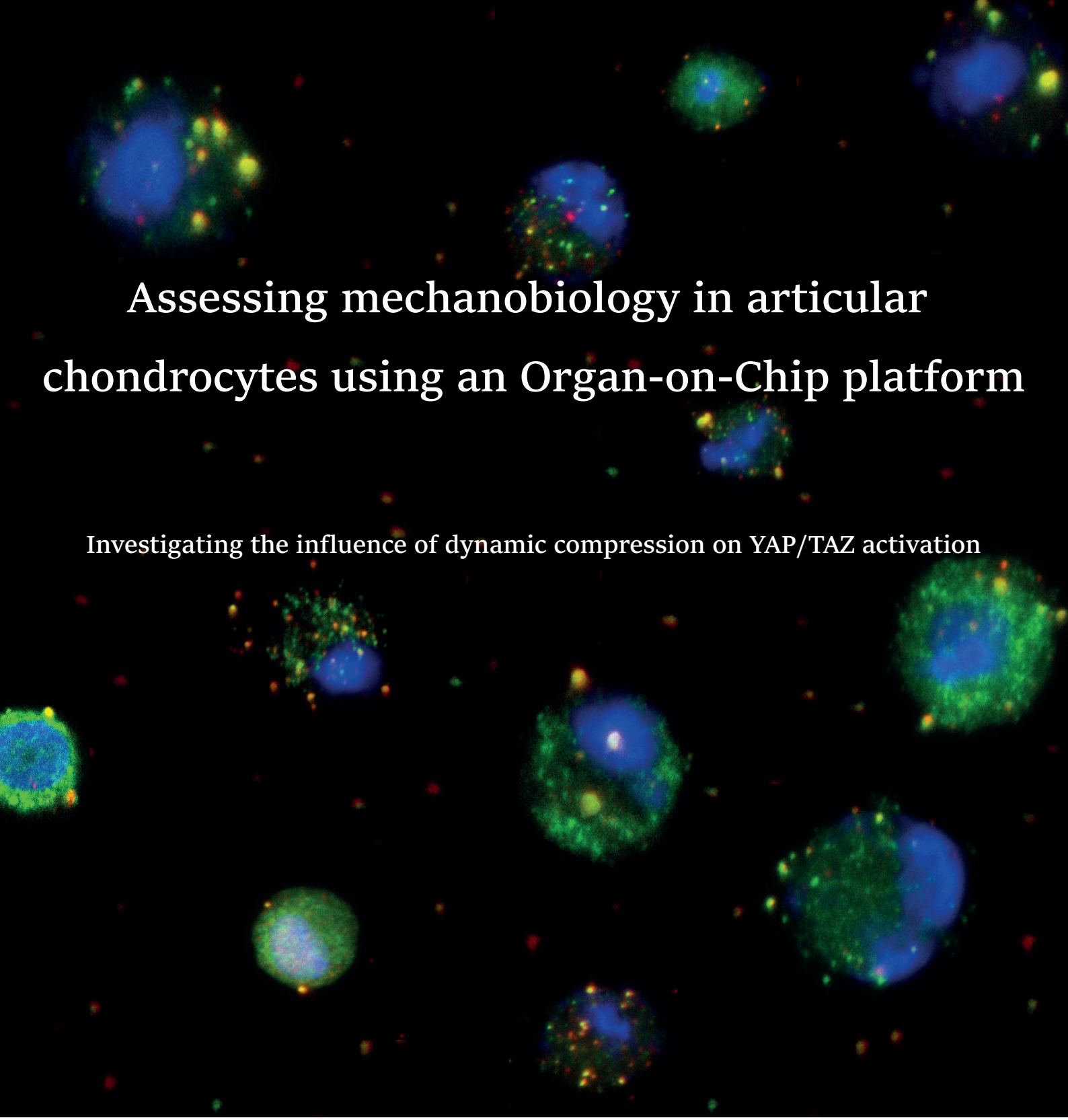

Assessing mechanobiology in articular chondrocytes using an Organ-on-Chip platform

Investigating the influence of dynamic compression on YAP/TAZ activation

Rosemarie Wijngaarden

A thesis presented for the degree of Master of Science

UNIVERSITY OF TWENTE.

Assessing mechanobiology in articular chondrocytes using an Organ-on-Chip platform

Investigating the influence of dynamic compression on YAP/TAZ activity

Rosemarie Wijngaarden

A thesis presented for the degree of Master of Science

Biomedical Engineering

Bioengineering Technologies

Graduation Committee

Chairman Prof.Dr. Marcel Karperien

Professor, Developmental Bioengineering

Supervisor Dr. Liliana Moreira Teixeira Leijten

Assistant Professor, Advanced Organ Bioengineering and Theurapeutics

Daily Supervisor Dr. Nuno Araújo Da Cunha Gomes

Postdoc, Developmental Bioengineering

External Member Dr.Ir. Jeroen Rouwkema

Associate Professor, Department of Biomedical Engineering

UNIVERSITY OF TWENTE.

Developmental Bioengineering (DBE)

Enschede, the Netherlands

09-01-2023

Abstract

Osteoarthritis (OA) is one of the most prevalent degenerative joint diseases in the Netherlands associated with pain and disability and the incidence is expected to rise rapidly. No treatment is available yet due to a lack of knowledge about the initiation and progression of the disease, as well as a representative research model. Physiological joint loading is necessary for matrix homeostasis and has proven beneficial for attenuating cartilage degradation during OA progression. The mechanobiology behind this could provide invaluable information about homeostatic processes and reveal potential targets for therapeutics, however it is not well understood yet. YAP/TAZ (YAP) transcriptional co-activators have shown potential in attenuating cartilage degradation in OA tissues, but controversy exists about the mechanism. This thesis investigates YAP activity upon dynamic compression in normal and pathological conditions, to eludicate part of the mechanobiology in chondrocytes.

A Cartilage-on-Chip platform was used to deliver physiological dynamic compression (300mbar, 1 Hz, 1hr/day) onto human primary chondrocytes embedded in agarose. YAP and SMAD protein nuclear translocation was measured using immunofluorescence to estimate the nuclear-to-cytoplasmic ratio over time and in addition of pro-inflammatory cytokines IL-1β and TNF-α. Additionally, gene expression was measured of matrix components and targets downstream of YAP-SMAD2/3 and YAP-SMAD1/5/9 complexes.

The results reveal that YAP, SMAD2/3 and SMAD1/5/9 nuclearisation does not increase upon physiological dynamic compression. CTGF was however upregulated, showing some influence of compression on the transcriptional activity of YAP. Nuclear YAP and SMAD2/3 increased upon addition of cytokines, while compression attenuated the nuclearisation of SMAD2/3. In contrast, nuclear SMAD1/5/9 only increased upon addition of cytokines in combination with compression. Downregulation of CTGF and Pai-1 in both pathological conditions demonstrates the influence of inflammation on the transcriptional activity of YAP-SMAD2/3. Furthermore, compression in pathological condition presents attenuated upregulation of MMP13, which could potentially be related to increased nuclear YAP.

This thesis concludes no direct influence of dynamic compression on YAP phosphorylation and nuclear translocation, however an influence on transcriptional activity of YAP is suggested by the data. This research could be continued by investigating the role of YAP in Extracellular Matrix (ECM) development or homeostasis, using YAP inhibitors and stimulators to regulate YAP expression and activity. Future experiments should increase the biological sample size and also include a physiologically relevant ECM to assess the role of mechanotransduction on YAP activation. The findings of this thesis show the possibility to investigate mechanobiology in the Cartilage-on-Chip platform, which could be applied to other signalling pathways involved in matrix homeostasis and potentially study the development of OA.

Samenvatting

Artrose is één van de meest voorkomende degeneratieve gewrichtsziektes in Nederland die gepaard gaat met pijn en bewegings beperkingen en naar schatting groeit het aantal patiënten snel. Er is nog geen behandeling beschikbaar vanwege een gebrek aan kennis over de initiatie en progressie van de ziekte en een representatief onderzoeksmodel. Fysiologische belasting is nodig voor kraakbeen homeostase en kan de afbraak van het kraakbeen tijdens de progressie van artrose vertragen. De mechanobiologie hierachter wordt echter nog niet goed begrepen, wat waardevolle informatie zou kunnen opleveren over homeostatische processen en potentiële doelwitten voor medicatie. YAP/TAZ (YAP) transcriptie co-activatoren tonen potentie om kraakbeen afbraak in artrose te verzwakken, maar dit mechanisme wordt nog niet goed begrepen. In deze thesis wordt de actviteit van YAP onderzocht bij dynamische compressie in normale en pathologische condities, om meer te weten te komen over de mechanobiologie in chondrocyten.

Een Cartilage-on-Chip platform is gebruikt om fysiologische dynamische compressie (300 mbar, 1 Hz, 1 uur per dag) toe te passen op menselijke primaire chondrocyten ingebed in agarose. De nucleaire translocatie van YAP en SMAD-eiwitten is gemeten met behulp van immunofluorescentie, om de nucleair-cytoplasmatische verhouding te schatten over de tijd en in aanwezigheid van pro-inflammatoire cytokines IL-1β en TNF-α. Bovendien is de genexpressie geanalyseerd van matrix componenten en genen geassocieerd met YAP-SMAD2/3 en YAP-SMAD1/5/9-complexen.

De resultaten tonen dat YAP, SMAD2/3 en SMAD1/5/9 nuclearisatie niet toeneemt door fysiologische dynamische compressie. Upregulatie van CTGF toont aan dat compressie invloed had op de transcriptie-activiteit van YAP. Wanneer cytokines werden toegevoegd, toonde YAP en SMAD2/3 een verhoogde nuclearisatie in statische condities, terwijl SMAD2/3-nuclearisatie minder werd in aanwezigheid van compressie. Daarentegen nam SMAD1/5/9-nuclearisatie alleen toe door compressie in aanwezigheid van cytokines. De afname van CTGF en Pai-1 in beide pathologische condities toont aan dat ontsteking invloed heeft op de transcriptie-activiteit van YAP-SMAD2/3. Bovendien zorgde compressie voor minder upregulatie van MMP13 in pathologische condities, wat potentieel gerelateerd is aan de toename YAP nuclearisatie.

Deze thesis concludeert dat er geen directe invloed is van dynamische compressie op de fosforylatie en nucleaire translocatie van YAP, maar de data suggereert wel een invloed op de transcrip-tieactiviteit van YAP. Dit onderzoek kan worden voortgezet door te kijken naar de rol van YAP in de ontwikkeling of homeostase van de Extracellulaire Matrix (ECM), door gebruik te maken van YAP-remmers en -stimulators. In vervolg experimenten moet de sample grootte worden verhoogd en een fysiologisch relevante ECM worden gecreëerd om de rol van mechanotransductie op de activatie van YAP te beoordelen. De bevindingen van deze thesis laten zien dat het mogelijk is om mechanobiologie te onderzoeken in het Cartilage-on-Chip platform, wat kan worden toegepast op andere signaalpaden die betrokken zijn bij matrix homeostase en mogelijkde ontwikkeling van OA.

Contents

List of abbreviations

Abbreviation	Meaning
AB	Antibody
Acan	Aggrecan
ADAMTS	A Disintegrin and Metalloproteinase with Thrombospondin motif
BSA	Bovine Serum Albumin
CoC	Cartilage-on-Chip
Col2	Collagen II
CTGF (CCN2)	Connective Tissue Growth Factor
Cyr61 (CCN1)	Cysteine-Rich angiogenic inducer 61
DAPI	4',6-diamidino-2-phenylindole
DMEM	Dulbecco's Modified Eagle Medium
ECM	Extracellular Matrix
EDTA	Ethylenediaminetetraacetic acid
ELISA	Enzyme-Linked Immunosorbent Assay
FA	Focal Adhesion
FAK-Src	Focal Adhesion Kinase- Steroid Receptor Coactivator
FBS	Fetal Bovine Serum
GAG	Glycosaminoglycan
HEK	Human Embryonic Kidney
HPC	Human Primary Chondrocytes
HTRA1	HtrA Serine Peptidase 1
IκB	Nuclear factor of kappa light polypeptide gene enhancer in B-cells inhibitor
Ihh	Indian Hedgehog
IKK	IκB kinase
IL-1β	Interleukin-1 beta
IL-6	Interleukin-6
ITS-premix	Insulin-Transferrin-Selenium premix

Abbreviation	**Meaning**
LATS	Large Tumor Suppressor kinase 1
LMP	Low Melting Point
MAP-ERK	Mitogen-activated protein kinase - Extracellular signal-regulated kinase
MMP	Matrix Metalloproteinases
MST	STE20-like serine/threonine kinase
N/C	Nuclear-to-Cytoplasmic ratio
Nf-κB	Nuclear factor kappa light chain enhancer of activated B-cells
OA	Osteoarthritis
OoC	Organ-on-chip
PBS	Phosphate-buffered saline
PCAD	Projected Cell Area Deformation
PCM	Pericellular Matrix
PDMS	Polydimethylsiloxane
Rho/ROCK	Rho/Rho-associated protein kinase
ROI	Region of Interest
RT-qPCR	Reverse Transcription quantitative Polymerase Chain Reaction
SD	Standard Deviation
SMAD	Suppressor of Mothers against Decapentaplegic
TEAD	Transcriptional enhancer factor TEF
TGF-β	Transforming Growth Factor beta
TNF-α	Tumor Necrosis Factor alpha
Vinc	Vinculin
Wnt	Wingless-related integration site
YAP	Yes-Associated Protein/WWTR1

Chapter 1

Introduction

Osteoarthritis (OA) is the most common degenerative joint disease and is associated with pain and disability. In the Netherlands, OA is one of the two most prevalent joint diseases affecting about 480.000 in 2017[1, 2]. The incidence of OA is rising rapidly, as the population is aging and obesity rates are rising globally[3, 4]. OA is characterised by progressive degeneration of the cartilage matrix, synovial inflammation and changes in subchondral bone structure[5]. Symptoms are chronic pain, swelling, joint instability, stiffness and radiographic jointspace narrowing, causing decreased mobility and decreased quality of life[6]. The initiation of the disease has been linked to mechanical overloading of the joint, while moderate physical activity is linked to cartilage homeostasis[7]. Age is by far the highest risk factor for developing OA, next to knee injury and obesity[8].

Due to a lack of understanding of the initiation and progression of OA, treatment is limited to surgery and pain mitigation[4]. This however does not cure the disease and current pain medication can increase the risk of cardiovascular morbidity[3]. In addition, cartilage has little regenerative capability which renders the disease progressive. OA research is partially dependent on (limited) tissue samples acquired from joint replacement surgeries, providing some insight into OA, typically relating to late stages of the disease[9]. Current research is focused on the role of joint loading on OA progression and the role of inflammation in cartilage degeneration, focusing on end end-point outcomes, namely the matrix remodelling. However, little insight into the inner mechanics of mechanotransduction which triggers matrix remodelling is gained. Therefore, further research into mechanobiology is necessary to unravel the role of different pathways in matrix remodelling and how these can be utilized in OA treatment. In this thesis, an organ-on-chip platform is used to apply mechanical compression on chondrocytes in an agarose matrix to study the response of mechanotransduction pathways in normal and pathological conditions.

1.1 Biological background

1.1.1 Articular cartilage

Articular cartilage is hyaline cartilage that covers the surface of load-bearing joints and protects the underlying structures[10]. In addition, it provides a smooth, lubricated surface causing a low frictional coefficient during movement. It mainly consists of extracellular matrix (ECM) and does not contain blood vessels, lymphatics, and nerves, which limits its healing capacity. The structure can be divided into three zones with a different organisation and composition of matrix components, Figure 1.1. The superficial zone provides resistance against sheer, tensile, and compressive forces, while the deeper zone mainly absorbs and dissipates compressive forces.

Chondrocytes are the only cellular component present in articular cartilage, making up only 2% of the total volume [10]. They maintain matrix homeostasis by regulating cartilage synthesis and cartilage degradation, through anabolic and catabolic metabolism respectively. Chondrocyte morphology, spatial organization, and ECM turnover is dependent on their location in the cartilage, Figure 1.1. A chondrocyte together with its pericellular matrix (PCM) make up a chondron, the micromechanical and metabolically active functional units of articular cartilage[11]. Because cartilage lacks vascularisation, chondrocytes thrive on anaerobic metabolism. The PCM encapsulates the chondrocyte and transduces biochemical and biomechanical signals, regulates fluid flow, and prevents the cells from migrating and cellular contact[10]. Signalling between cells is enabled by mechanical loads, ion influx and biochemical signalling.

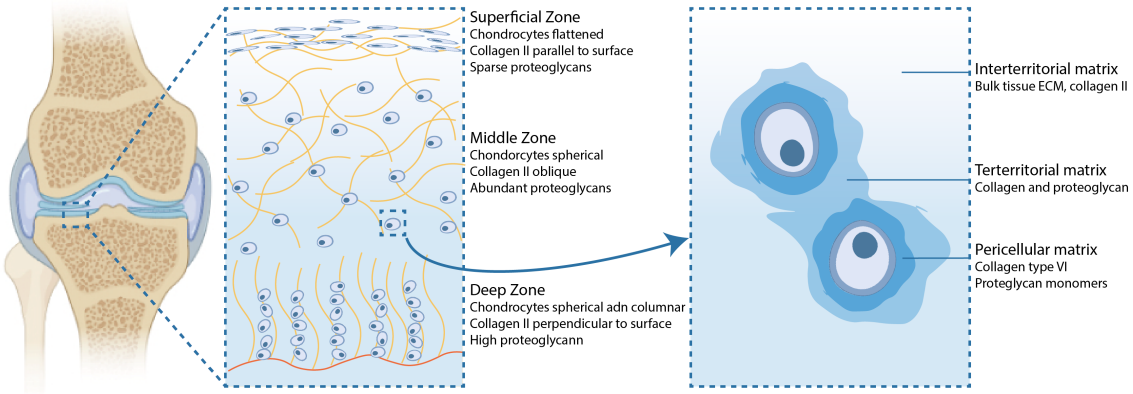

Figure (1.1) Articular cartilage zones and composition. The articular cartilage covers the surface of load bearing joints such as the knee. The structure can be divided into three zones, the superficial, middle and deep zone, with a characteristic composition of ECM and chondrocyte orientation. Collagen II is the most abundant collagen and aggrecan the most abundant proteoglycan present in articular cartilage. The chondrocyte microenvironment can also be divided into three zones, the closest being the pericellular matrix, followed by the territorial matrix and interterritorial matrix, which is the bulk tissue ECM. The PCM is characterised by collagen type VI and perlecan, but also contains hyaluronan, biglycan and fibronectin. The territorial matrix is composed of a fine collagen fibril network. Inspired by [11, 12], made with biorender

The main components found in articular cartilage are water, collagen, and proteoglycan [11]. Collagen II forms fibrils and fibers intertwined with proteoglycan aggregates, that provide stability through hydrogen bonds. Collagen type I, IV, V, VI, IX and XI are less present and stabilise the collagen II network. Proteoglycan consist of a linear protein core with negatively charged glycosaminoglycan (GAG) chains covalently attached to form combs. The main proteoglycan, aggrecan, can form large proteoglycan aggregates with hyaluronic acid, which give cartilage its water retaining ability. Ions are dissolved in the water, enabling their transport through movement of fluid through the matrix upon compressive loading. Carti-

lage homeostasis is maintained by a balance between the synthesis of these matrix components and matrix degrading enzymes. The main enzymes involved are matrix metalloproteinase (MMP) and a disintegrin and metalloproteinase with thrombospondin motif (ADAMTS), degrading collagen and proteoglycan respectively.

Normal physiological loading is well tolerated by the joints and during higher loading regimes, the cartilage surface and ECM absorb and dissipate the impact forces to protect the joint[11]. Loading forces in the knee joint range from 2-4 times body weight during daily activities and scale linearly with increased body weight[13, 14]. Other forces acting on the joint are shear stress induced by synovial fluid flow, hydrostatic pressure from fluid retained by proteoglycans, and osmotic stress from changes in solute concentration[15, 16]. The smoothness of the superficial zone provides a low frictional coefficient that enables relative movement of opposing cartilage surfaces with minimal wear. For this movement, the collagen network provides resistance to tensile and shear forces generated by sliding of the condyles in the knee-joint. The proteoglycan meshwork in the deeper cartilage zones provides resistance to compressive forces. Negatively charged GAG chains act as a sponge that retains water when unloaded. The force from compressive loading pushes the water out, generating a large drag force that provides compressive resilience.

Physiological joint loading is needed to maintain cartilage homeostasis, regulating distribution of cartilage thickness and providing important stimuli for increasing cartilage synthesis [11]. Dynamic compression stimulates matrix synthesis, while static or hyperphysiological loading inhibits matrix synthesis and can cause a shift toward catabolic activity leading to matrix degradation[17, 18]. Loading cartilage with higher forces has also shown to increase articular cartilage thickness[19]. Furthermore, development of degenerative diseases is associated with dramatic changes in cartilage metabolism.

The influence of mechanical stimulation on matrix remodelling by chondrocytes has been studies widely, showing a dependency on frequency, magnitude, and duration of applied forces[20, 21, 22]. In general, static compression is found to downregulate gene expression of aggrecan and collagen II, while dynamic compression upregulates these genes, as did hydrostatic pressure. When introducing shear stress, proteoglycan and collagen II are upregulated compared to dynamic compression [20, 21, 23]. These studies provide information about the resulting ECM production after stimulation, however the signalling behind this response remains elusive.

1.1.2 Mechanobiology of articular chondrocytes

Mechanotransduction maintains joint health by regulating the transcriptional activity in chondrocytes[24]. It can be defined as the whole process of converting mechanical stimuli into biochemical signals, which are transported into the nucleus and elicit a cellular response. This process is initiated by proteins on the membrane that act as mechanosensors, such as ion channels, integrins, and receptors[25].

The PCM plays an important role in mechanotransduction by regulating the forces acting upon the chondrocyte. The matrix gradually reduces the compressive loading force and regulates hydrostatic pressure and fluid flow to maintain homeostasis [24]. Additionally, the PCM deforms upon mechanical loading, causing the release of ECM-bound proteins or decreasing the distance between these proteins and the cell membrane surface, which enables ligand-receptor binding[20, 24, 26]. Some proposed mechanotransduction pathways regulating chondrocyte behaviour include integrin signalling[27], purinergic signalling[28], calcium signalling[29], pri-

mary cilia [30, 31], and biochemical signalling such as Ihh, Wnt, MAP-ERK, Hippo, and TGF-β pathways[24, 25, 32, 33]. The latter two have received more interest in OA research lately.

Hippo signalling

Yes-associated protein (Yap) and WWTR1 (TAZ) are transcriptional co-activators that regulate gene transcription[25]. Upon activation, they migrate inside the nucleus and interact with other transcription factors, regulating cell fate, organ size, and wound healing. Because YAP/TAZ (YAP) do not contain a DNA binding motif, transcriptional activity is dependent on these other transcription factors and their interaction depends on the phosphorylation status[34]. Phosphorylation sequesters the YAP complex to the cytoplasm in an inactive state, which is regulated mainly through the Hippo pathway. In this Hippo pathway, MST1/2 phosphorylates LATS1/2 which in turn phosphorylates YAP, enabling nuclear transport, Figure 1.2. Several other pathways interact with the Hippo pathway by inhibiting or stimulating LATS, or by directly phosphorylating YAP[35]. Some of these pathways respond to mechanical stimuli such as substrate stiffness, giving YAP a role in mechanotransduction[36, 37].

Integrin is a transmembrane protein that forms a physical link between the ECM and the intracellular cytoskeleton. The tail of integrin provides docking sites for proteins that recruit more proteins to form focal adhesions (FA). The size and amount of FAs formed correlate to the force felt by the cell, through ECM tension and stiffness, which increase the recruitment of stress fibers to the FA[25]. The cytoskeleton acts as a second messenger by regulating the tension inside the cell and effectively the cell shape, maintaining tensional homeostasis by altering the cytoskeletal architecture and shuttling proteins into the nucleus. YAP is one of these mechanosensitive proteins that travels along the cytoskeleton fibers into the nucleus upon stiff substrates or low cell densities[36, 39]. Suggested pathways that influence this process are either Hippo dependent, or Hippo independent, Figure 1.2[37]. The Rho/ROCK pathway

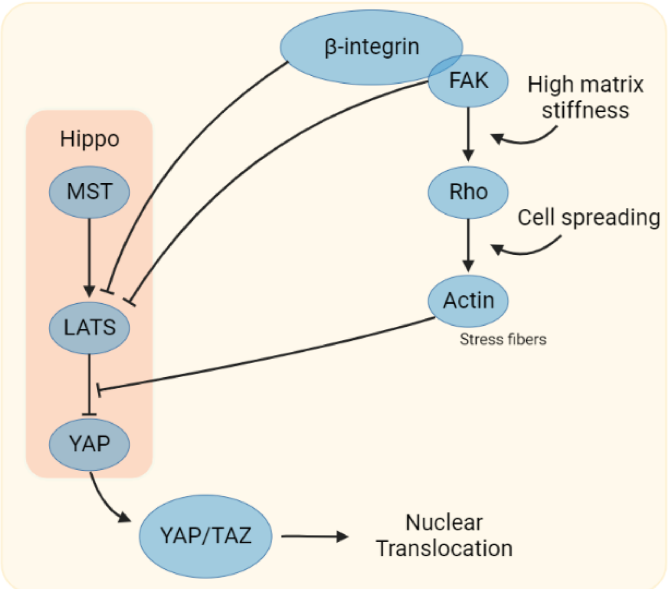

Figure (1.2) Overview of YAP regulation through Hippo pathway and mechanical cues. In the Hippo pathway, MST phosphorylates LATS, which then phosphorylates YAP and inhibits nuclear translocation of the YAP complex. Cell-matrix interactions stimulate YAP activity through focal adhesions, by inhibiting LATS (Hippo-dependent) or by directly influencing YAP phosphorylation through Rho/Rock (Hippo-independent). Rho stimulates actin cytoskeleton stabilisation, which promotes YAP nuclearisation. Mechanical cues such as high matrix stiffness and increased cell spreading stimulate YAP nuclearisation. The pointed arrow indicates stimulation while the flat arrow indicates inhibition. Image inspired by [38, 35, 37], made with biorender

mediates cytoskeleton stability and shows regulation of YAP nuclearisation[25], in a Hippo-independent way. LATS1/2 phosphorylation of YAP is inhibited through FAK-Src upon cell-cell contact, in a Hippo dependent way[38, 35]. In turn, YAP controls the transcription of genes involved in FA formation and cytoskeleton stability, as a response to the microenvironment [40, 41].

Transforming Growth Factor beta (TGF-β) signalling

TGF-β is a family of proteins involved in tissue homeostasis, including TGF-β and bone morphogenetic proteins (BMPs). These growth factors interact with a set of receptors, forming specific complexes sensitive to the different family members[42]. TGF-β members can activate multiple intracellular signalling pathways, which are either R-SMAD-dependent or independent[33]. In the canonical (R-SMAD-dependent) pathway, two groups are distinguished: SMAD2/3 and SMAD1/5/9 (or SMAD1/5/8), Figure 1.3. Upon phosphorylation, these groups complex with co-SMAD4 enabling nuclear translocation and subsequently gene transcription. TGF-β induces phosphorylation of SMAD2/3 which in chondrocytes is associated with ECM synthesis, anti-hypertrophy, and anti-inflammation. BMP induces SMAD1/5/9 phosphorylation, which is associated with hypertrophy and bone formation and is regarded as the antagonist of SMAD2/3 signalling. To maintain cartilage homeostasis, a balance between these pathways is needed [26].

Some of the components of the TGF-β signalling pathway are directly linked to the cytoskeleton, suggesting a role in mechano-transduction[26]. TGF-β is often used in chondrocyte culture to enhance matrix production[43], however the effect of gene transcription may depend on the process of chondrogenesis[21]. In addition, physiological loading of cartilage has shown increased SMAD2/3 nuclearisation, presenting a regulatory role in chondrocyte maturation and matrix production[44]. However, high concentration of TGF-β has been associated with SMAD1/5/9 signalling causing MMP13 expression and cartilage degradation[5]. Furthermore, TGF-β has an important anti-inflammatory role by inhibiting catabolic pathways including Nf-κB[33].

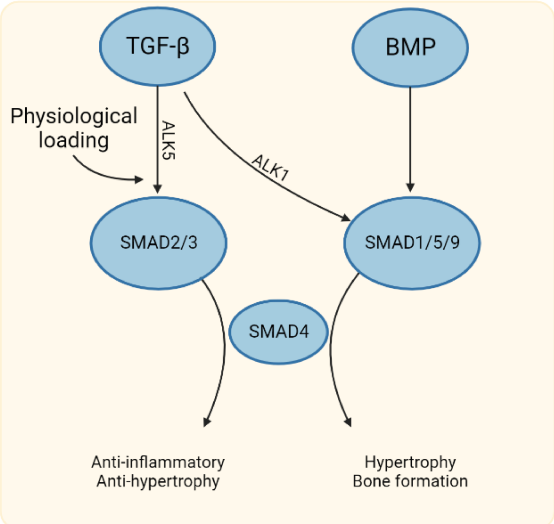

Figure (1.3) Overview of TGF-β/SMAD signalling. TGF-β phosphorylates SMAD2/3 through the ALK1 receptor, which enables interaction with SMAD4 resulting in nuclearisation. SMAD2/3 transcription is associated with anti-hypertrophy and anti-inflammation. SMAD1/5/9 is the antagonist of SMAD2/3, which is regulated by BMP, a member of the TGF-β family. SMAD1/5/9 transcription is associated with hypertrophy and bone formation. TGF-β can also cause SMAD1/5/9 phosphorylation through the ALK5 receptor in presence of stresses such as inflammation or abnormal loading. A balance between both pathways is needed to maintain cartilage homeostasis. Image inspired by [33], made with biorender

1.1.3 Pathophysiology of osteoarthritis

Mature chondrocytes exist in a somewhat resting state causing homeostatic cartilage turnover. In contrast, OA is characterised by proliferation, hypertrophy, remodelling of the cartilage matrix, vascularisation and focal calcification[5]. These processes are regulated by growth factors and cytokines causing upregulation of matrix degenerative enzymes. Of these enzymes, MMP13 and ADAMTS5 are most widely researched in association with OA[9, 43]. Mechanical overloading can release latent growth factors and cytokines bound to the ECM and shift the metabolic activity towards cartilage degeneration. As a result, the PCM thins which reduces its protective ability, increasing this imbalance even more[16, 45]. Once the collagen matrix degrades, disease progression is irreversible[46].

Additionally, OA is characterised by inflammation. Inflammation can reprogram chondrocytes toward hypertrophic differentiation and stimulate catabolic metabolism through Nf-κB[6, 47]. Without stimulation, Nf-κB activity is inhibited by IκB proteins. Pro-inflammatory cytokines such as IL-1β and TNF-α and stress-like responses from abnormal loading trigger the activation of NF-κB through the canonical pathway [48], Figure 1.4. When activated, Nf-κB causes cartilage degradation through upregulation of MMPs and ADAMTSs and stimulation of inflammatory pathways[49, 50].

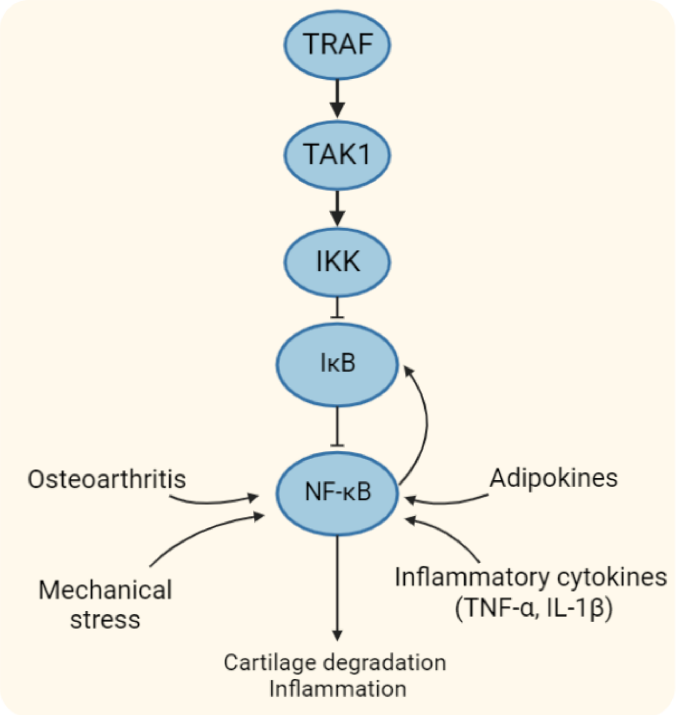

Figure (1.4) Overview of the canonical Nf-κB pathway. Without stimulation, Nf-κB is retained in the cytoplasm by IκB proteins. When stimulated, IκB kinases (IKK) promotes degradation of IκBs and Nf-κB is released. Active Nf-κB is involved in upregulation of cartilage degrading enzymes and stimulation of inflammatory pathways. Nf-κB also regulates IκB transcription in a negative feedback loop. Through the canonical pathway, regulation occurs through TRAF and TAK1. Activation of Nf-κB is associated with many stimuli including inflammation and abnormal mechanical stress. Image inspired by [49], made with biorender

An increased risk of developing OA is associated with age and obesity[8]. Age induces several changes in cartilage which influence functionality[17]. With age, fewer chondrocytes are found in the superficial zone and more in the deeper zones, affecting cartilage homeostasis and disrupting the smooth surface of the superficial zone. Additionally, matrix hydration decreases which reduces friction between the interstitial fluid and the aggrecan meshwork, resulting in increased cartilage stiffness[9]. Lastly, a shift in TGF-β signalling is seen from SMAD2/3 to SMAD1/5/9 resulting

in cartilage degradation[51]. Obesity both increases the mechanical load upon the load-bearing joints and introduces chronic inflammation. An increase of $\frac{1}{2}$ kilo is associated with a fourfold increase in knee compressive forces [14]. In addition, chronic inflammation continuously triggers the catabolic metabolism resulting in cartilage degradation.

1.2 Regulation of YAP transcriptional activity

As mentioned above, YAP do not possess a DNA binding motif and therefore depend on other transcription factors to initiate gene transcription, some are summarised in Figure 1.5. Most reported are interactions with the TEAD family, promoting cell growth, proliferation and transformation[34]. Target genes of this complex are CTGF- and CYR61, which are involved in ECM remodelling[52].

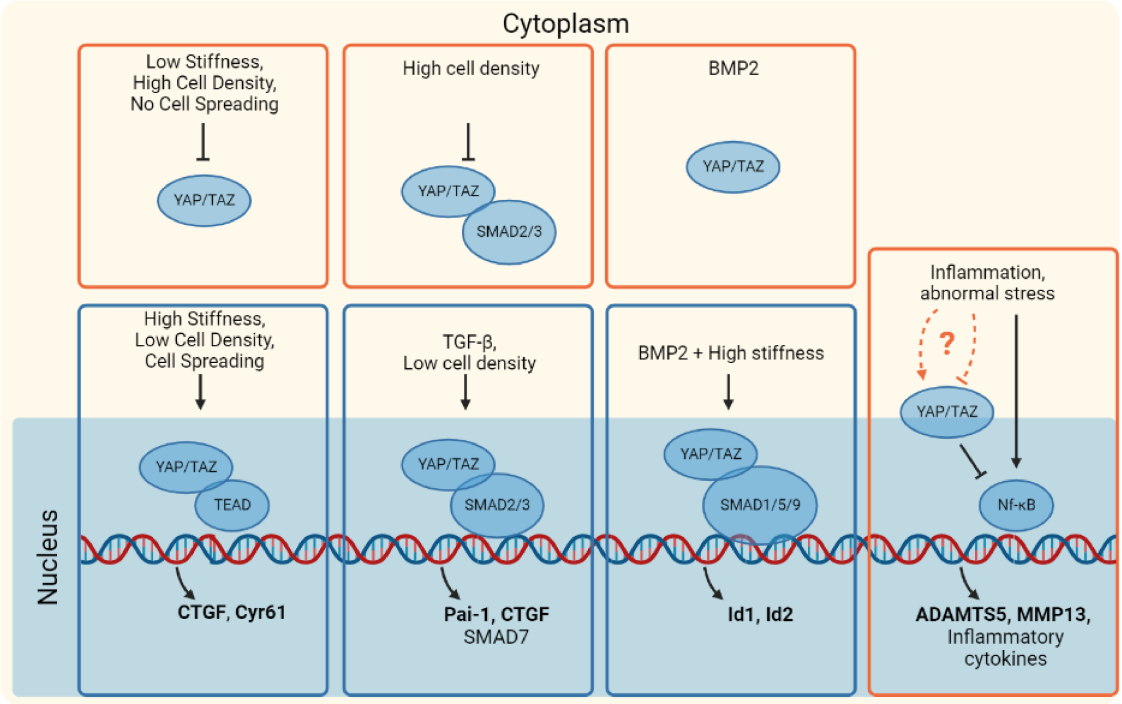

Figure (1.5) Overview of suggested interactions from literature between YAP and transcription factors, downstream target genes and induced response upon stimuli. Most reported are YAP interactions with members of the TEAD family, playing a role in cell growth, survival and transformation. Downstream targets of YAP-TEAD complex are CTGF and Cyr61 which are involved in matrix remodelling. Interaction with the SMAD family has been suggested to regulate the nuclearisation or cytoplasmic sequestering of the YAP-SMAD complex, depending on the present stimuli. Some targets downstream of YAP-SMAD2/3 are Pai-1, CTGF and additionally SMAD7. SMAD7 inhibits SMAD2/3 activity, which introduces a negative feedback loop. Downstream targets of YAP-SMAD1/5/9 include Id1 and Id2. Finally, a suggested pathway is shown upon inflammation. YAP attenuates Nf-κB induced cartilage degradation in OA models, suggested through inhibition of TAK1 ubiquitination of IKK. However, controversy exists in the literature about the influence of YAP in atttenuating cartilage degradation in OA. Genes in bold are targets used in this thesis, inspired by [34], made with biorender

YAP-SMAD interactions have also been identified in response to mechanical cues. Depending on cell density, more YAP-SMAD2/3 complex was found in the nucleus (low cell density) or sequestered in the cytoplasm (high cell density)[53]. The latter suppresses TGF-β signalling through upregulation of SMAD7, inhibiting SMAD2/3 activity[34]. Upon abnormal mechanical stimulation, YAP-SMAD2/3 nuclearisation may induce HTRA1 which contributes to joint degradation[54]. Furthermore, induction of TGF-β showed that YAP regulates bone remodelling in osteocytes[55]. Additionally, YAP is sequestered upon soft substrates, while stiff substrates stimulate YAP nuclearisation. In the presence of BMP2, YAP-SMAD1/5/9 co-localises in the nucleus to initiate osteogenic differentiation[56].

In human Embryonic Kidney (HEK) cells, inflammatory cytokines revealed activation of the Hippo pathway, resulting in sequestering of YAP in addition to proteasomal degradation of YAP[47]. While this interaction was not present in chondrocytes, overexpression of YAP did demonstrate inhibition of Nf-κB mediated degradation of cartilage in OA mice. Suggested was that upregulation of YAP could therefore be a potential treatment to attenuate cartilage degradation in OA. In contrast, another study showed that YAP was upregulated in OA tissues, suggesting that inhibition of YAP with siRNA could prevent cartilage degradation in OA[57].

The discussed literature shows the influence of substrate stiffness, cell volume, cell density and inflammation on the activation of mechanotransduction pathways Hippo-YAP and TGF-β/SMAD. However, the influence of dynamic mechanical compression on these pathways remains elusive[37]. Furthermore, conflicting observations were presented about the potential of YAP to attenuate cartilage degradation in OA cartilage. Investigating the inner mechanics of these pathways could give information on how YAP activity is related to cartilage homeostasis and how they can potentially be used in therapeutic interventions for OA.

1.3 *In vitro* models

To study mechanobiology in chondrocytes *in vitro*, direct cartilage biopsies from animal tissues or patient donors are used to keep the native ECM intact, but are limited in availability. To simulate this, chondrocytes are cultured in porous hydrogel matrices, where they produce ECM over time to resemble the physiological microenvironment. Chondrocytes embedded in an agarose matrix have shown ECM production and have been used to study the effect of mechanical stimulation on chondrocytes[58, 59, 60]. These cartilage or hydrogel samples are mechanically compressed to deliver static or dynamic loading, often using bulky equipment or set-ups with limited control over the environment.

Another way to study mechanobiology *in vitro* is using Organ-on-Chip (OoC) technology, which allows better control over the microenvironment. These chips are designed to simulate a simplified, microscale model of a tissue or organ, by integrating 3D cell culture and microchannels to deliver nutrients or stimulants. By using smart designs, actuation can be integrated using valves or membranes[61, 62]. Due to the microscale technology, low sample volumes are needed which can be beneficial for limited tissue samples. Additionally, isolation and simplification of tissue allows better control over parameters, therefore enabling the study of specific cellular responses to applied stimuli without interference of other tissues. Furthermore, multiple OoCs could be connected to study interaction between tissues, which is of interest for OA as it is a multiple-organ disease.

Previous work in the group resulted in a monolithic Cartilage-on-Chip (CoC) device which uses a 50 µm thin vertical membrane for easier fabrication and analysis, Figure 1.6[23]. Multiple designs (1-3 actuation chambers) deliver either homogeneous compression or multimodel compression, the latter introducing bulk shear forces. Cells are seeded inside a culture chamber (1260 µm long, 4000 µm wide and 250µm high) and nutrients are supplied through a medium channel. Using physiological compression (300 mbar pressure), upregulation of collagen II was detected, which increased more when using the multimodel actuation. A PCM resembling physiolgical thickness (5 µm) was obtained after 15 days of culture and stimulation. Further findings show that a static culture period of 7 days after seeding decrease pro-inflammatory cytokines concentrations (IL-6, IL-1β, and TNF-α) and that the

direction of stimulation influences the organisation of proteins[23]. This platform will be used in this thesis to study mechanotransduction upon mechanical compression in chondrocytes.

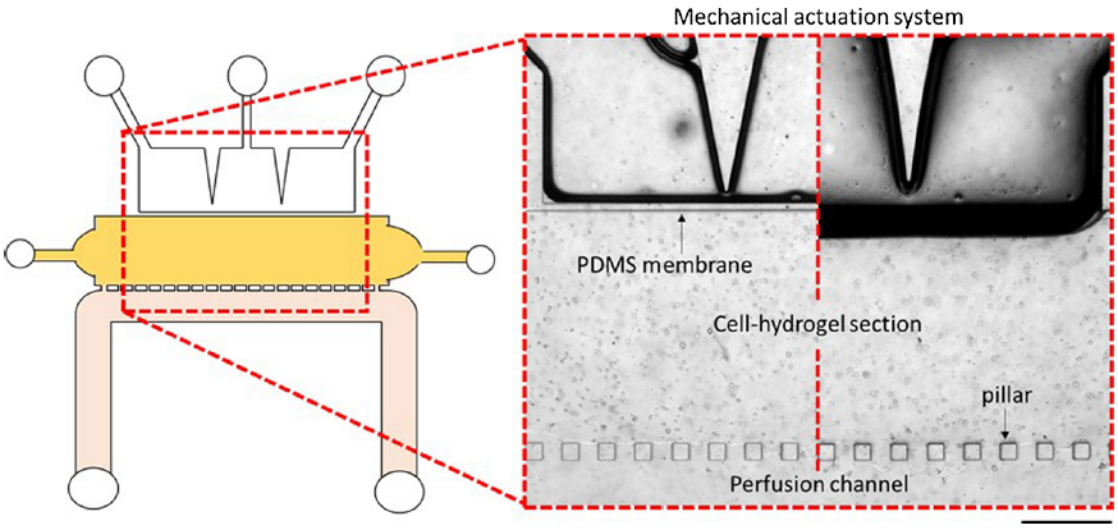

Figure (1.6) Cartilage-on-Chip platform (left) design of the chip with (top) actuation chamber (middle) culture chamber and (bottom) medium channel. The culture chamber is separated from the other chambers by a thin membrane (50 µm) and pillars. The actuation chamber can be pneumatically actuated to deform the membrane (right), which compresses the hydrogel-cell mixture and delivers compressive forces onto the cells (left uncompressed, right compressed). Scalebar = 500 µm. [23]

Chapter 2

Research Aim & Approach

2.1 Aim and objectives

YAP has been identified as a key player in mechanotransduction, however the regulatory role of mechanical loading on YAP activity has not been investigated yet. The aim of this thesis is to assess the influence of dynamic mechanical compression on YAP activation in chondrocytes. This relationship will be investigated by analysing YAP activation, together with several suggested mechanotransduction pathways influencing YAP activation.

The focus of this study is uncovering more about the role of YAP in mechanotransduction, as it has shown the potential to attenuate cartilage degradation in OA[47, 57, 63]. To understand this mechanism, the following objectives were formulated:

- Investigate whether dynamic compression affects YAP activation in chondrocytes.
- Determine the influence of dynamic compression in a pathological condition on the regulation of YAP in chondrocytes.

Several pathways have been identified as mechanosensitive and have been linked to YAP activity, such as FAs and release of ECM bound TGF-β followed by the activation of SMAD pathways. The response of these individual components upon dynamic compression, in combination with the activation of YAP and ECM production by chondrocytes, will be analysed to achieve these objectives.

Connections between YAP, FAs and SMAD pathways have been investigated before in static conditions, by focusing on substrate stiffness, cell density and cell area. The interaction of these proteins upon dynamic compression has not yet been explored. As physiological loading is needed to maintain cartilage homeostasis and has shown beneficial for attenuating cartilage degradation during OA, investigating these pathways upon physiological loading could provide new insights into pathway crosstalk and cell behaviour, which could prove beneficial for OA research.

2.2 Research approach

The research approach of this thesis is focused on investigating the response of YAP and SMADs in chondrocytes upon dynamic mechanical compression. This is realised by investigating the influence of pressure magnitude, time, and induced inflammation on protein activation and matrix remodelling.

A CoC platform is used to apply dynamic compression to human primary chondrocytes (HPC) embedded in agarose. A compressive load of 300 mbar is applied to simulate loading during walking, which delivers a strain to the cells (3.5-10%) comparable to physiological loading[64]. This regime is repeated for 1 hour per day at 1 Hz to simulate the pace of a normal walking gait. As control, chips are kept static throughout the experiment. Pro-inflammatory cytokines IL-1β and TNF-α are added to the medium to simulate OA[65].

To give insight into binding of YAP with other transcription factors, gene expression of downstream targets is measured through RT-qPCR: CTGF and Cyr61 for YAP-TEAD transcription, Pai-1 for YAP-SMAD2/3 transcription, and Id2 for YAP-SMAD1/5/9 transcription. In addition, the TGF-β1 concentration is measured through an ELISA to give insight into TGF-β-SMAD signalling. Furthermore, matrix remodelling is analysed through immunofluorescence to investigate the production of collagen II and aggrecan, RT-qPCR to analyse both matrix components in addition to matrix degrading enzymes MMP13 and ADAMTS5, and Alcian Blue staining to analyse GAG production.

Hypothesised is that dynamic compression increases the nuclearisation of YAP, similar to a stiff substrate condition. If this is the case, an increased N/C ratio is expected and upregulation of CTGF and Cyr61 through YAP-TEAD transcription. Additionally, it is expected that nuclear SMAD2/3 is increased upon dynamic compression as shown before in the literature, therefore increased N/C ratio and upregulation of CTGF and Pai-1 is expected through YAP-SMAD2/3 transcription. Because nuclear SMAD1/5/9 is not increased upon physiological dynamic compression, no change in N/C ratio and gene transcription of Id1 and Id2 through YAP-SMAD1/5/9 is expected. Furthermore, it is hypothesised that in presence of inflammation, the TGF-β pathway shifts from SMAD2/3 to SMAD1/5/9 activation, increasing YAP-SMAD1/5/9 transcription and thus upregulation of Id1 and Id2. Expected is that physiological dynamic compression will attenuate this effect.

This thesis can be divided into two sections. The first is focused on optimising analysis protocols and validation of the mechanical actuation protocol. These results are discussed and used to perform the experiments in the second part, which consists of several mechanical actuation experiments to look at protein activation over time and in a simulated pathological condition.

Chapter 3

Methods

3.1 Fabrication of Cartilage-on-Chip device

To make the CoC device, a SU-8-on-silicon mould was used[23]. Using soft-lithography, PDMS pre-polymer was mixed with curing agent (Sylgard 184, Dow Corning, USA) with a weight ratio of 20:1 and poured on the wafers, thoroughly degassed and cured at $65°C$ for 24 hours. In the same manner, a thin PDMS layer was fabricated in a petri dish. The chips were cut and punctured with 1 and 2 mm diameter punchers. To assemble the device, the PDMS layer was bonded to a glass slide and in turn the chip onto the glass-PDMS layer using plasma treatment (Cute plasma oven, Femto Science, South Korea) or (Harrick Plasma, Anadis, Netherlands). The devices were then placed in the oven at $65°C$ for 24 hours before use.

3.2 Cell culture of human Primary Chondrocytes

Healthy looking HPC were thawed and cultured in T175 flasks (Cellstar®, Greiner bio-one, Germany) in chondrocyte proliferation medium (DMEM with 10% fetal bovine serum (FBS), 100 UmL^{-1} penicillin and 100 gmL^{-1} streptomycin, 0.2 mM ascorbic acid 2-phosphate, 0.1 mM non-essential amino acids, 4 mM proline). To passage the cells, they were washed with PBS (1x) and trypsinised using a trypsin-EDTA 0,25%/0.1 M solution and reseeded in a new flask at 1 million cells per 175 cm^2. Cells were used at passage 4 for the experiments.

3.3 Seeding of cells in chips

To inject the cells into the CoC device, 4% w/v agarose (UltraPure Low Melting Point agarose, Invitrogen) was diluted in PBS (1x) and heated until dissolved. This was kept in a $50°C$ water bath to cool down for at least one hour. Meanwhile, the culture flask with cells was washed with PBS (1x) and trypsinised. The cell concentration was determined with trypan blue and the EVE cell counter and adjusted to 3 million cells/mL and kept at $37°C$. The agarose was mixed with the cell suspension resulting in a final concentration of 1.5 million cells/mL in 2% w/v agarose to inject into the chips. Chondrocyte proliferation medium was added to the medium channel approximately 1 minute after injection into the device. This medium was later replaced and refreshed every day with chondrocyte differentiation medium (DMEM with 100 UmL^{-1} penicillin and 100 gmL^{-1} streptomycin, 1x insulin-transferrin-selenium (ITS)-premix, $50gmL^{-1}$ ascorbic acid 2-phosphate, 40 gmL^{-1} proline, 1x sodium pyruvate, 20 $ngmL^{-1}$ TGF-β3, $10^{-7}M$ dexamethasone).

Medium of the previous day was collected from the medium channel by pooling medium from 6 chips and frozen at $-80°C$ until analysis.

3.4 Mechanical stimulation of chips

Mechanical stimulation was applied as shown in Figure 3.1. The chips were kept static for 5 days after seeding prior to mechanical stimulation. Unless mentioned otherwise, the chips were mechanically stimulated on day 5 to 9, and again on day 12 with 300 mbar positive pressure at a frequency of 1 Hz, which was done for 1 hour each day. The medium was refreshed before stimulation. For stimulation, chips were connected through 18 gauge needles and Tygon tubing (MasterFlex™ Microbore tubing, Thermo Fisher Scientific) to a microfluidic manifold (7 port manifold, Darwin Microfluidics, USA). The manifolds were connected to Flow EZ™ (Microfluidic flow controller, pressure output from 0 to 2000 mbar, Fluigent, France), which are controlled by Fluigent and Microfluidic Automation tool software (AiO-All in One, Fluigent). Actuation was validated for each chip by looking if the membrane moved using a camera (RS PRO USB Digital Microscope, RS Components, UK).

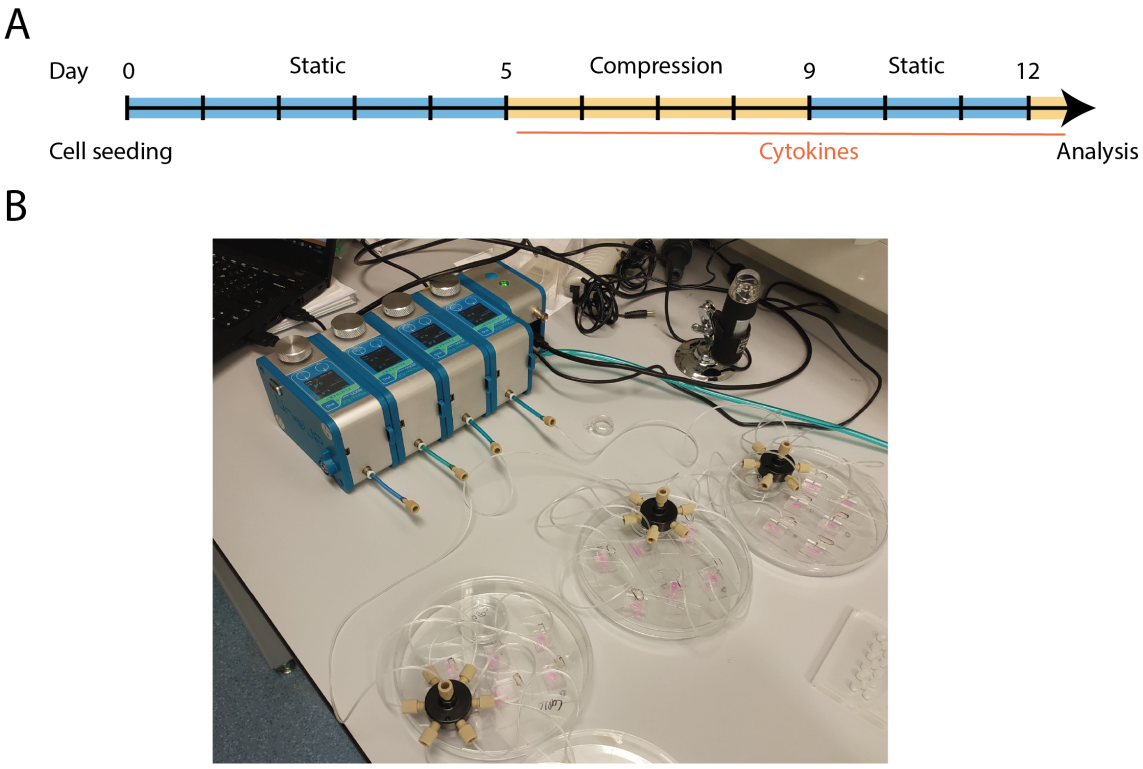

Figure (3.1) Stimulation protocol over 12 days. Cells are seeded inside chips on day 0 and kept static until day 5. On day 5 to day 9 mechanical stimulation is applied with 300 mbar compression at 1 Hz for 1 hour per day. From day 10 to 11, no stimulation is applied. On day 12, chips are stimulated and after stimulation processed for analysis. For pathological conditions, IL-1β and TNF-α are added to the medium from day 5 to day 12. Chondrocyte differentiation medium is used for the whole protocol and refreshed on day 1-2, 5-9 and on day 12.

3.5 Live/dead assay

To determine the viability of chondrocytes in the chips, the hydrogel samples were retrieved from the PDMS and stained for 10-15 minutes with calcein AM (green/live) and ethidium homodimer-1 (red/dead) (Thermo Fisher Scientific) and imaged on the EVOS FL microscope (Thermo Fisher Scientific). Images were taken of three separate areas per chip at 10x magnification. These images were analysed in ImageJ

software using a self-made script to automate cell counting (S3). In this script, the brightness was adjusted between 0-50 and a Gaussian Filter applied with radius 1 to reduce out-of-focus signal. To measure overlap, imagecalculator with 'both' was used. Particle analysis counts the number of red, green, and overlapping cells. The total number of green stained cells is regarded as live cells and the number of red cells diminished by overlapping cells regarded as dead cells. If this results in a negative value, the number of dead cells is taken as 0. Viability was determined by

$$\text{Viability in } \% = \frac{\text{Live cells}}{\text{Live} + \text{Dead cells}}$$

3.6 Induced pathology

To induce a pro-inflammatory-like state in the chondrocytes, cytokines IL-1β and TNF-α were used. First, a viability test was done on a monolayer of HPC. On day 2-5 of culture, 2, 5 or 10 ng/mL of both cytokines was added to the medium. A viability staining was performed on day 6 (S2.6). From this data it was decided to use 5 ng/mL cytokine concentration for the actuation experiments, which were added to the medium on day 5-12, Figure 3.1.

3.7 Immunofluorescence

Samples were retrieved from the chips approximately 1 hour after mechanical stimulation. They were washed 3x with PBS (1x) and fixated with 10% formalin (Sigma Aldrich, USA) in 10 minutes. For the washing steps, the liquid was taken up with a tissue by carefully touching the hydrogel to remove excess liquid. After fixation, samples were washed 3x with PBS and permeabilised with 0,25% TritonX-100 (Sigma Aldrich) in PBS for 30 min, washed again 3x with PBS and blocked in 1% Bovine Serum Albumin solution (BSA, Sigma Aldrich) in PBS for 1 hour. Next, primary antibody (AB) was diluted in BSA and incubated overnight at 4°C. The next day, samples were washed 3x with PBS and incubated with secondary antibody in BSA for 1-1,5 hours. This procedure was repeated if a double staining was implemented following 3 washes and incubation with DAPI (4',6-diamidino-2-phenylindole, 1:100 dilution rate, Thermo Fisher Scientific) for 15 minutes. Finally, the samples were washed 3-5x with PBS and stored at 4°C until further use. Antibodies and dilutions are listed in Table 3.1 and were validated in monolayer culture of HPC, Figure S2.4. Immunostaining of chip samples was done on µ-Slide 4 Well chambered polymer coverslip (Ibidi, Germany).

3.8 Imaging and analysis

Samples were imaged on a Carl Zeiss Confocal microscope (Zeiss LSM880, Carl Zeiss Microscopy, Germany) using a Zeiss C-Apochromat 40x Water immersion objective (NA=1.2, WD=0.28 mm) and Zeiss Immersol™ W 2010 (N_e=1,334 at 23°C23). For this, samples were dried with a tissue to keep the gels in place and then hydrated with a drop of 100-200 µL PBS to prevent shrinking of the sample during imaging. Each dye was imaged in a separate track, with a pinhole of 49.2 (DAPI 1.56 AU, AF488 1.24 AU, and AF647 1.00 AU). Gain and laser power were adjusted as needed for each sample. First, an overview was made using a tile-scan of the entire sample at one z-position of the gel (between 1100 and 1400 nm height), by turning the stage

Table (3.1) List of primary and secondary antibodies and dilutions used for immunofluorescence staining of chip samples.

Target	Antibody	Dilution	Source
Primary Antibodies			
Acan	Mouse-anti-aggrecan	1:100	Abcam (ab3778)
Col2	Rabbit-anti-collagen II	1:100	Abcam (ab34712)
Phalloidin	Alexa Fluor™ 488 Phalloidin	1:40	ThermoFisher (A12379)
SMAD2-3	Rabbit-anti-SMAD2/3	1:200	CellSignal (D7G7)
p-SMAD1/5/9	Rabbit-anti-p-SMAD1/5/9	1:200	CellSignal (D5B10)
Vinc	Rabbit-anti-vinculin	1:100	Abcam (ab129002)
YAP	Mouse-anti-YAP	1:100	Santa Cruz (sc101199)
Secondary Antibodies			
AF488	goat-anti-rabbit AF488	1:200	Invitrogen (a11008)
AF647	donkey-anti-mouse AF647	1:200	Abcam (ab150107)

such that the top of the image represents the membrane side of the sample. This overview was used to choose the positions of individual cells in the gel, which were imaged using a z-stack of 21 slices (1 µm spacing). Random cells throughout the sample were chosen for static conditions and for mechanically stimulated conditions, only cells between the top and middle of the gel were considered.

Focal Adhesion analysis

FAs form the connection between the cytoskeleton and ECM and are often involved in mediating signalling pathways. FAs consist of many proteins and can be imaged by choosing one of these proteins. In this study, vinculin was used to visualise the FAs and phalloidin to stain F-actin as validation. Images were analysed in ImageJ using several plugins as described in [66]. Particle analysis was done to measure the area and number of FAs. For 3D stacks, first a z-projection is made by summing the images which is converted to 8-bit for analysis.

Nuclear-to-Cytoplasmic ratio

Because transcription factors translocate into the nucleus, determining the fraction of protein inside the nucleus compared to the cytoplasm could give an indication of the activity. Stacks of single cells were analysed with ImageJ plugin Giani which allows batch analysis of 3D stacks[67]. This software segments nuclei and cells in stacks and generates masks. These masks are then used to measure the fluorescence intensity inside the nucleus and cytoplasm separately, which are used to calculate the N/C ratio using

$$\text{Nuclear/Cytoplasmic ratio} = \frac{\text{Nuclear Mean Fluorescence}}{\text{Cytoplasmic Mean Fluorescence}}$$

Giani was used with: Nuclear Radius for Simple Centroid Detection = 9 µm; Quality of Simple Nuclear Centroid Detection = 3; Filter Radius for Nuclear Channel = 1 µm; Threshold Method for Nuclear Segmentation = Default; Nuclear Volume Marker selected; Filter Radius for Cell Channel = 0.5 µm; Threshold Method for Cell Segmentation = Default; Cell Volume Marker selected. For the pathological conditions, Nuclear radius for Simple Centroid Detection was incresaed to 10 µm and Quality of Simple Nuclear Centroid Detection decreased to 1.

3.9 RNA extraction, cDNA synthesis and RT-qPCR

Samples were retrieved from the device directly after mechanical stimulation and 3 hydrogels were pooled for 1 sample. Unless mentioned otherwise, total RNA was obtained using the RNeasy Micro Kit (cat. Number 74004, QIAGEN, Germany). Samples were lysed using 350 µL RLT Buffer and homogenised by pipetting through a 26G needle. This was followed by the protocol described by the supplier, with an additional washing step with 80% ethanol. Quality and purity of extracted RNA was assessed using the NanoDrop™2000 spectrophotometer (Thermo Fisher Scientific). Samples were stored at $-80°C$ until further processing. Next, cDNA was synthesised with the iScript cDNA synthesis kit (Bio-Rad, USA) using the whole extracted RNA samples. RT-qPCR was performed using SensiMix™ SYBR® & Fluorescein Kit (Bioline, UK) on a CFX Connect Real-Time System (Bio-Rad). A table representing all primers can be found in Table 3.2. Efficiency was determined for validated primers (S2.3) and data was normalised to RPS18. Previously validated primers were assumed to have an efficiency of 100% and amplification of 2.

Table (3.2) Primers used for qPCR, 5' > 3'. * indicates primers of own design

Gene	Forward	Reverse
RPS18	TGAGGTGGAACGTGTGATCA	CCTCTATGGGCCCGAATCTT
YAP1 *	GCAGTTGGGAGCTGTTTCTC	GCCATGTTGTTGTCTGATCG
CTGF- (CCN2) *	GTTTGGCCCAGACCCAACTA	CTTCTTCATGACCTCGCCGT
Pai-1 *	CTCTCTCTGCCCTCACCAAC	GTGGAGAGGCTCTTGGTCTG
Id2 *	CGTGAGGTCCGTTAGGAAAA	ATAGTGGGATGCGAGTCCAG
hACAN	AGGCAGCGTGATCCTTACC	GGCCTCTCCAGTCTCATTCTC
Col2A1	CCAGATGACCTTCCTAGGCC	TTCAGGGCAGTGTACGTGAAC
MMP13	TCCTGATGTGGGTGAATACAATG	GCCATCGTGAAGTCTGGTAAAAT
ADAMTS5	TGGCTCACGAAATCGGACA	GGAACCAAAGGTCTCTTCACAGA
Col10A1	GCAACTAAGGGCCTCAATGG	CTCAGGCATGACTGCTTGAC

3.10 Calculation of Projected Cell Area Deformation and Gel Displacement

HPC were cultured on chip and kept static until day 5. On day 5, two chips of each CoC design (1, 2 or 3 chambers) were stimulated with 300 mbar compression at 1 Hz for 1,5 hours and imaged on an inverted microscope (IX51, Olympus, Japan) equipped with a camera (ORCA-flash, 4.0 LT, Hamamatsu Photonics, Japan). After this, one chip of each design was additionally stimulated with 500 mbar compression at 1 Hz for 30 min. This was done assess if there is a difference between the pressure magnitudes and designs. Timed image sequences were made at 250 ms intervals for 5 seconds. For each chip, two areas near the membrane and two areas near the pillars were imaged to measure the difference between these areas. From every image sequence, two images were selected to measure the area of static cells and two images to measure the same cells but in a compressed state. For every cell, a region of interest (ROI) was drawn with the circle tool on ImageJ around each cell three times to account for human error. The projected cell area deformation (PCAD) is calculated by

$$\text{Projected cell area deformation } [\%] = abs\left(\frac{\text{Static cell area - Compressed cell area}}{\text{Static cell area}}\right)$$

The absolute value is considered as the ROI is drawn as a circle, where a flattened cell results in a larger diameter which causes an increased cell area. These values should thus be considered relative values. The gel displacement is determined by the central X and Y coordinate of the cells inside the gel.

3.11 TGF-β1 ELISA

Medium from 6 chips was pooled together for one sample of approximately 15 µL and stored at $-80°C$ until further processing. Human/Mouse TGF-β1 Uncoated ELISA(Cat Number 88-8350, Invitrogen, USA) was used to determine the concentration of TGF-β1 in these samples, following manufacturers' protocol. First, it was validated that the TGF-β1 concentration from these low volume samples were measurable S2.10, were results showed a detectable concentration in only part of the samples. Because of this, the dilution of the sample as stated in the manufacturers' protocol (10x dilution) was reduced. To achieve this, samples were diluted with 25 µL PBX (1x) and acid-activated using 8 µL 1N HCl followed by 8 µL 1N NaOH, resulting in a 3,7x dilution. Absorption was measured in VarioscanLUx (Thermo Fisher Scientific) at 450 and 570 nm. A TGF-β1 concentration curve was determined by subtracting ELISA/ELISASPOT Diluent (1x) blank from the TGF-β1 dilution series and fitting a linear curve. Samples were corrected using medium samples retrieved from chips without cells.

To normalise the data, quantitation of DNA was done by QuantiFluor® dsDNA (Promega, Netherlands). For this, three static chips were pooled for one sample and lysed using CDP* lysis buffer ($0.1MKH_2PO_4$, $0.1MK_2HPO_4$, and 0.1% Triton X-100 with pH 7.8). Samples were incubated with lysis buffer for 1 hour at RT on a shaker and after stored at $-30°C$. For quantitation, samples were added to a plate directly from the lysate and measured together with Lambda dsDNA standard diluted in 1x TE buffer. Fluorescence was measured at 504 nm_{Ex}/531 nm_{Em} using Perkin Elmer Victor3 1420 Multilabel Plate Counter (Perkin Elmer, USA). DNA content standard curve was determined by subtracting the 1x TE buffer blank from the dilution series and fitting a linear curve. Samples were corrected using a no-cell control sample.

3.12 Alcian Blue staining

Alcian Blue and Fast Red solutions (Sigma Aldrich) were filtered before use. Samples were dried with a tissue and incubated for 30 min with Alcian Blue, washed with tap water and incubated for 8 minutes with Fast Red. Next, samples were washed 3x with tap water and fixated under a coverslip and sealed with nail polish before imaging on the NanoZoomer (Hamamatsu Photonics). Mean intensity was determined by measuring 10 areas in the hydrogel in between cells and normalised to a white area outside the sample. Conditions were compared to a no-cell control.

3.13 Graphs and statistical analysis

All data was visualised with Prism (GraphPad Software, Dotmatics, USA). Mean values are expressed with standard deviation (SD). Statistical analysis was conducted using ordinary one-way ANOVA, multiple comparison testing the mean, non-paired, with Tukey 99% confidence. For all experiments, HPC originating from

one donor were used (N=1 biological replicates). The analysed samples are therefore considered pseudoreplicates.

Chapter 4

Optimisation of protocols

The results and discussion have been divided into two parts. This first chapter will discuss the results of experiments trying to optimise protocols and validate analyses for the used platform. These results will be discussed and decisions made regarding what experimental conditions to use in the following mechanical stimulation experiments. The next chapter presents the results of protein nuclearisation and ECM production over time and in pathological a condition, followed by a discussion of these results.

4.1 Results

4.1.1 Viability of cells seeded inside CoC and after dynamic compression

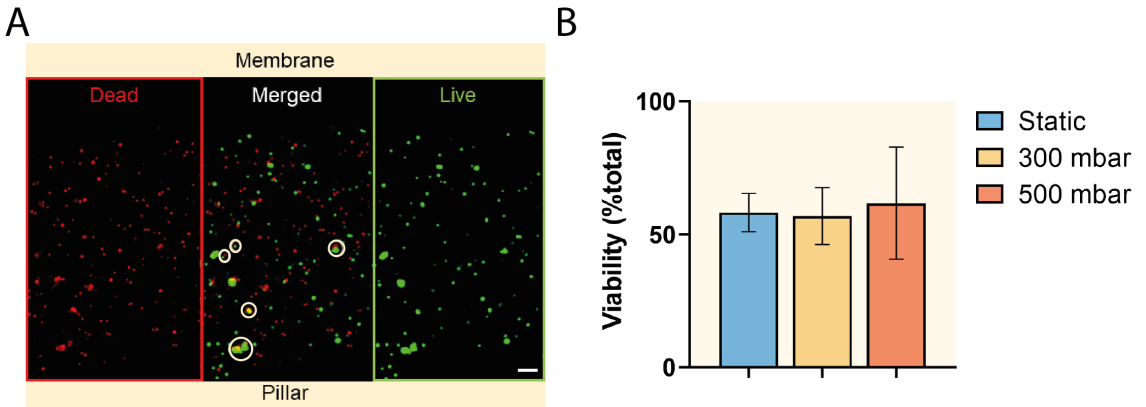

Figure (4.1) Viability of HPC after mechanical stimulation (A) Fluorescence image of chip sample after 300 mbar compression with circled cells showing both red and green signals, scalebar = 100 µm. (B) Viability of chondrocytes for static and compressed chips, N=3 chips, 3 areas measured per chip.

To seed the cells inside the CoC platform, the agarose is kept liquid at $50°C$. The agarose is then mixed with the cell suspension which is kept at $37°C$ and quickly injected into the chip before solidifying. To test if the cells remain viable throughout the experiment, a live/dead staining was performed, Figure 4.1. Some overlapping cells can be seen in both red and green channels, which is due to bleedthrough of the live staining into the red channel (S2.1). When calculating the viability, this is accounted for by taking the total number of dead cells as red stained cells diminished

by the number of overlapping cells, resulting in a viability of approximately 60% for each condition. This is quite low, however no significant decrease is seen after compression which suggests that compression of 300 and 500 mbar do not significantly affect cell viability.

4.1.2 Optimisation of RNA extraction method

Trizol extraction was not able to increase the quality nor purity of RNA extracted from agarose hydrogels. Because of the low cell content in the chips, around 1900 cells from 1.5 million cells/mL seeded inside a culture chamber of 1.26 µl (4000x1260x150 µm), it was investigated if TRIzol extraction could increase the RNA yield. For this, RNA was extracted using the TRIzol method (**Trizol**), the RNeasy Microkit (**Column**), and by combining both techniques (**Trizol+Column**), following protocols described in S1. Additionally, it was explored if agarase pre-treatment could increase the purity by degrading the agarose hydrogel around the cells before RNA extraction.

Figure 4.2A and B show a substantial increase of RNA concentration in all methods using Trizol, compared to the Column extraction. Because these values seemed unrealistic, it was examined if the Trizol method influences the measurements, shown in Figure 4.2C. The high RNA concentration measured in the no cell control of Trizol+Column indicate that Trizol affects the Nanodrop measurement. The no cell control of Column is considerably lower. Subtracting the control from the methods leaves 8,51 ng/µL RNA for Trizol+Column and 6,15 RNA ng/µL for Column. These resulting values indicate that the difference in extracted RNA between methods is low.

The absorption ratios still show high contamination for both techniques. Good

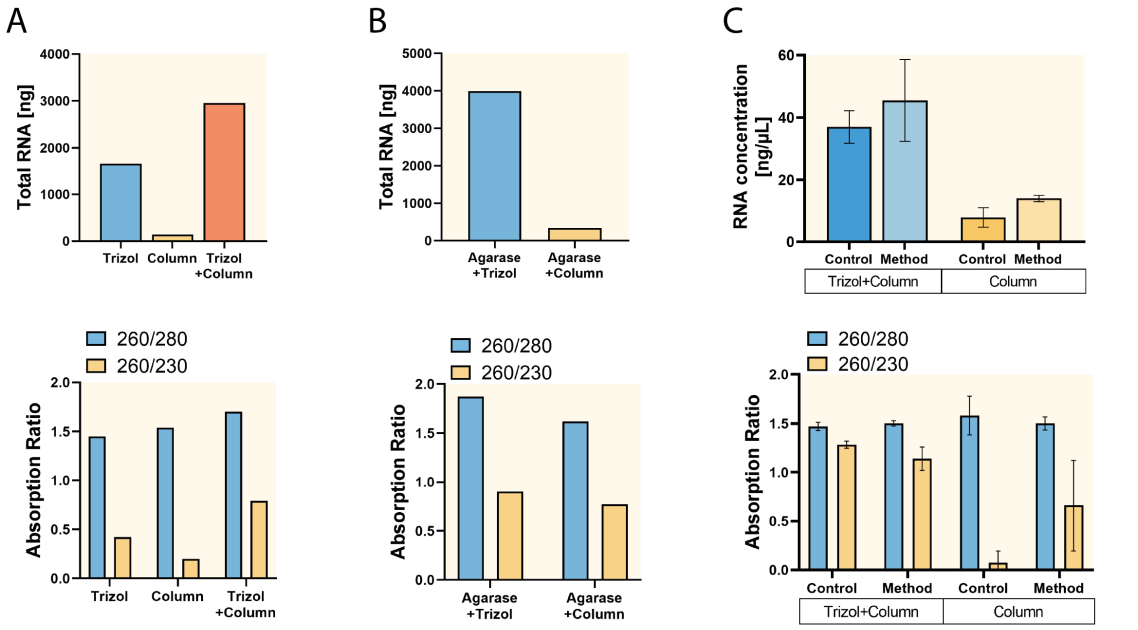

Figure (4.2) Comparison of different RNA extraction methods using droplets of agarose and HEK293 cells. The concentration of RNA is shown in the top graphs and absorption ratios in the bottom graphs for (A) Trizol, Column and combined methods and (B) Agarase pre-treatment before Trizol and Column methods. Both show a large increase of RNA concentration when using Trizol, N=1 chip. (C) Validation of contamination by comparing Trizol+Column and Column methods to a no cell control, with an additional 80% ethanol washing step to reduce impurities and lysate homogenisation through a 26G gauge needle to increase gel disruption. Trizol influences the concentration and purity measurement, N=3 chips. Note that no error bar is present in A and B because one sample per condition was tested.

quality RNA should show absorption ratios around 1.8-2.0 for 260/280 and 2.0-2.2 for 260/230, lower values indicate contamination with compounds absorbing around 280 and 230 respectively. Figure 4.2C together with the absorption spectra in S2.2 show high contamination around 230 nm for all techniques. In addition, extraction with TRIzol shows contamination at 270 nm which affects the 260 nm readout. Guanidine (iso)thiocyanate is present in both TRIzol and RLT buffer from the RNeasy Microkit and shows absorption at 230 nm, likely causing the contamination. From these results it was decided to continue using the Column method.

4.1.3 Detection of Focal Adhesions in a 3D hydrogel

No difference in FA formation was detected in chondrocytes upon different compression magnitudes, Figure 4.3. The immunofluorescence images

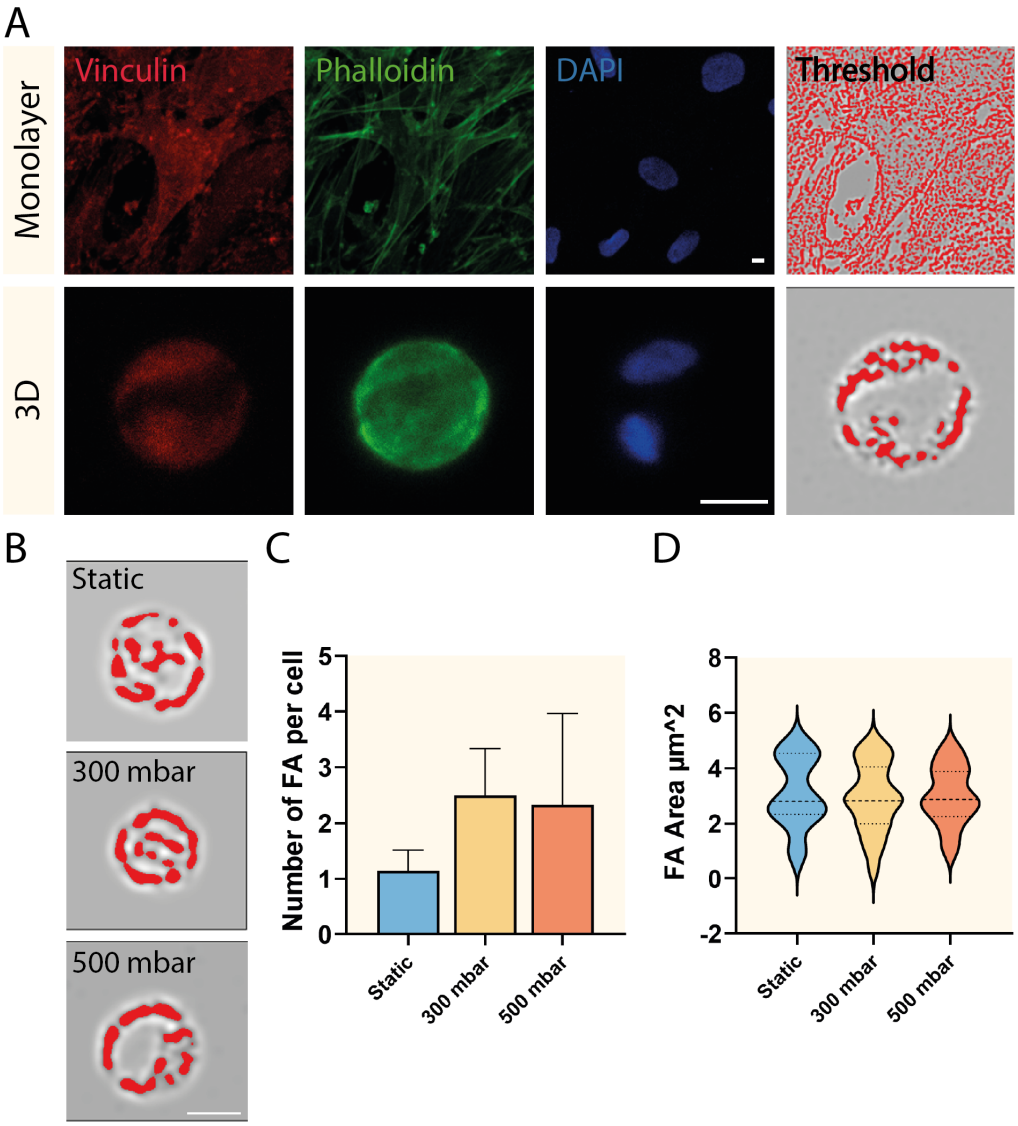

Figure (4.3) Detection of FAs in HPC (A) Immunofluorescence images of chondrocytes cultured in monolayer (2D) and chip (3D) for 14 days showing actin fibers and vinculin. The chip was stimulated with 300 mbar compression on day 7-11 and 12. The last image shows the processed red channel with threshold, illustrating what is analysed as FA (B) Threshold images of static and compressed conditions at day 14, showing FAs mainly on the edges of the cell. (C) Number of FAs per cell and (D) Mean area of FAs which both show similarity for all conditions, N=1 chip per condition, 9 cells measured per chip. Note that FBS was present in the chondrocyte differentiation medium during this experiment. Scalebar = 10 µm

show the difference of FA formation in cells cultured in monolayer and in 3D. In the monolayer culture, it was hard to isolate a single cell and its FAs, however the red thresholding shows a clear outline of the cell, which is were most of the FAs are expected to be formed. In Figure 4.3B representative images are shown for each condition, which look quite similar. Quantification of the FAs in chip samples reveal no significant difference in static and compressed conditions. Notably, not all FAs appear as isolated spots in the thresholding image, but rather as one larger area which was accounted for by only including areas <5 µm^2. This corresponds roughly to a diameter of 2.5 µm, which has been indicated by literature to be the maximum size of FAs detected in 3D[68]. Only a slight increase in the number of FAs per cell is present in the compressed conditions. The variation however is too large to be considered as a difference. Because of these results and the low amount of samples available, it was decided not to continue with this type of analysis in future experiments. Instead, Alcian Blue staining is used to indicate GAG production and immunofluorescence of collagen II and aggrecan to indicate ECM production.

4.1.4 Influence of chip design on dynamic compression of chondrocytes

Large variability was detected due to chip seeding quality , Figure 4.4B and statistical analysis in Table 4.1. Both 300 and 500 mbar compression do not show a difference in PCAD between cells near the membrane and cells near the pillar, between chip designs, and between compression magnitude. Additionally, Figure 4.4C reports no difference between increased compression magnitude. This data suggests that the cells do not undergo significant deformation at 1 Hz application of 300 and 500 mbar compression.

The difference between measures of cells near the membrane and cells near the pillar gives an indication of gel compression. The gel near the membrane should move more compared to the gel near the pillars, as the gel is obstructed by these pillars. 300 mbar compression shows no difference between gel displacement of cells near the membrane compared to cells near the pillars, while 500 mbar compression shows a significant difference for the 1 and 2 Chambers designs. When comparing the designs, the 2 Chambers design shows a larger gel displacement compared to 1 and 3 Chambers. The mean of all designs near the membrane reveal a slight increase upon 500 mbar compression, Figure 4.4E.

One observation that was often made in these chips was a gap between the agarose and the membrane (S2.7), which can cause an increase in gel displacement both near the membrane and the pillars. These gaps are formed either during the seeding procedure or after mechanical stimulation. During seeding, the agarose needs to be kept warm enough to stay liquid, therefore several chips are seeded after each other before medium is added to the medium channel to prevent drying of the agarose. If the time between seeding and adding medium is too long, the agarose can dry and shrink, thereby creating a gap. It can also be caused later after mechanical loading if the agarose at the pillar side breaks which affects the deformation upon loading (S2.7). An increased gap allows for more displacement compared to no gap, where the displacement is a result only from compression of the gel. The gel displacement in these graphs could therefore not only depend on the chip design, but also on the quality of the gel inside the chip. The low sample size used in this experiment (N=2 chips for 300 mbar and N=1 chip for 500 mbar) could explain the high variability between the 2 Chambers design and the other designs. For better comparison between these conditions, the experiment should be repeated

using more chips per condition.

To decrease the influence of the chip design in following experiment, chips with 3 actuation chambers were used for mechanical stimulation and chips with 1 and 2 chambers for static conditions. Furthermore, the quality of the chips was assessed before the first mechanical stimulation by looking at limited gap between PDMS and agarose and the quality of the membrane.

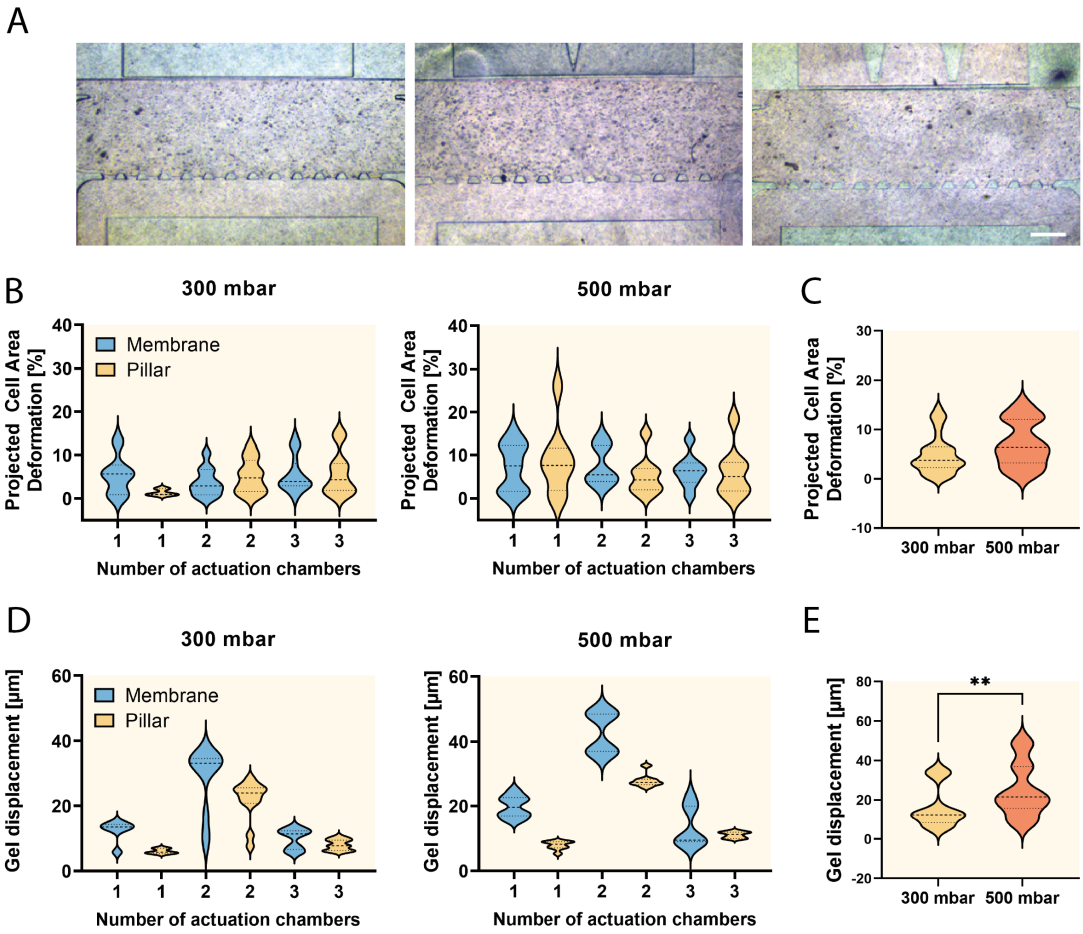

Figure (4.4) Comparison of CoC designs with 1, 2 or 3 actuation chambers during 300 and 500 mbar dynamic compression on day 5. (A) Microscope images of cells seeded inside the 1, 2 and 3 chambered design, scalebar = 100 µm. (B) and (C) PCAD of compressed cell area relative to static cell area (B) per chamber design for 300 and 500 mbar compression, looking at areas near the membrane or the pillars and (C) mean of all designs near the membrane. No difference is detected between conditions. (D) and (E) Gel displacement looking at cell movement between static and compressed states (D) per chamber designs for 300 and 500 mbar compression, statistical analysis presented in Table 4.1, and (E) mean of all designs near the membrane showing a difference between 300 and 500 mbar compression. N=2 chips for 300 mbar and N=1 chip for 500 mbar. Pvalues: $0.001 < P <= 0.01^{**}$

4.1.5 Influence of pressure magnitude on protein nuclearisation

A single dynamic compression session with 500 mbar increases nuclearisation of SMAD1/5/9. In an attempt to shorten the experimental protocol, YAP, SMAD2/3 and SMAD1/5/9 nuclear localization was estimated after only one dynamic compression session for 300 and 500 mbar, Figure 4.5. The immunofluorescence images illustrate the difference of SMAD1/5/9 between a lower N/C ratio for Static versus a higher N/C ratio for 500 mbar. For the latter condition a higher fluorescence intensity can clearly be seen in the nucleus. This difference is not present in the YAP and SMAD2/3 images (S2.8). Only the N/C ratio of SMAD1/5/9 is increased after one session of mechanical compression of 500 mbar. 300 mbar compression does not show any difference compared to static conditions.

Table (4.1) Statistical analysis comparing gel displacement in multiple chip designs over different pressure magnitudes, graphs shown in Figure 4.4D. Pvalues: $0.001 < P <= 0.01^{**}$, $0.0001 < P <= 0.001^{***}$, $P <= 0.0001^{****}$

Comparison of membrane to pillar in one design	300 mbar	500 mbar	
1 Chamber membrane vs. pillar	ns	****	
2 Chambers membrane vs. pillar	ns	****	
3 Chambers membrane vs. pillar	ns	ns	
Comparison between designs	**300 mbar**	**500 mbar**	
1 Chamber vs. 2 Chambers	****	****	
1 Chamber vs. 3 Chambers	ns	ns	
2 Chambers vs. 3 Chambers	****	****	
Comparison between pressure magnitudes	**1 Chamber 500 mbar**	**2 Chambers 500 mbar**	**3 Chambers 500 mbar**
1 Chamber 300 mbar	ns	****	ns
2 Chamber 300 mbar	**	****	****
3 Chamber 300 mbar	****	****	ns

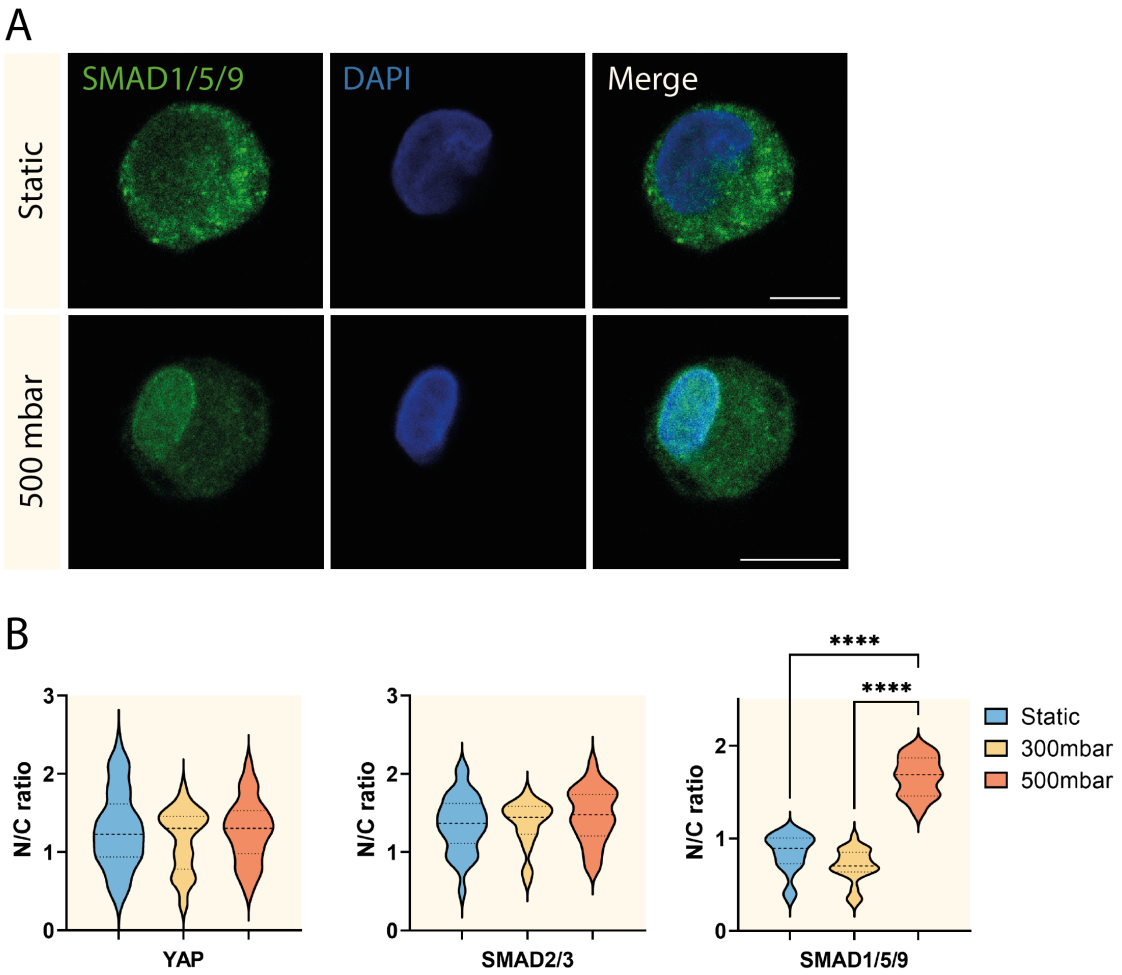

Figure (4.5) Influence of a single dynamic compression session of HPC with 300 or 500 mbar at day 5 compared to static condition. (A) Immunofluorescence images of single cells representative for SMAD1/5/9 AB for Static and 500 mbar condition (YAP and SMAD2/3 shown in S2.8), scale bar = 10 µm. (B) N/C ratio of YAP, SMAD2/3 and SMAD1/5/9, N=1 chip (SMADs) and N=2 chips (YAP), 19-36 cells analysed per chip. Pvalues: $P <= 0.0001^{****}$

4.2 Discussion

The aim of this part was to validate and optimise protocols to study mechanobiology using the Cartilage-on-Chip platform. Mechanical compression of chondrocytes seeded inside a hydrogel can simulate loading forces upon articular cartilage, similar to standing or walking. Physiological compression in articular cartilage enhances matrix production and helps maintain homeostasis, while hyperphysiological strain is associated with cartilage degradation[17, 18]. Loading of chondrocytes in a physiological (3.5-10% deformation) and hyperphysiological (5-25% deformation) range could be achieved by using homogeneous static compression of 300 and 500 mbar respectively[64]. Performing a similar experiment with dynamic compression at 1 Hz did not show a significant cell area deformation, suggesting that the cell area is not significantly influenced by dynamic compression. In consequence, dynamic compression is unlikely to activate mechanotransduction pathways associated with alterations in cell volume[60]. In contrast, gel displacement was increased upon stimulation with a higher pressure magnitude. This was however more likely caused by the chip seeding quality in this experiment, than by the pressure magnitude. Because the CoC platform uses a vertical membrane to apply compression horizontally to the gel, gaps between the hydrogel and the PDMS chip wall will have consequences for the forces acting upon the cells. Therefore, the compression force is reduced in some chips compared to others depending on the seeding quality, which introduces variability in the system. In comparison, mechanical compression is often applied vertically on agarose or cartilage discs [51, 58, 60, 69], these systems however have less control over the microenvironment and experimental parameters.

In this study, one session of hyperphysiological compression showed to increase the nuclearisation of SMAD1/5/9, but not upon physiological compression. Additionally, no change was seen in SMAD2/3 nuclearisation. Release of ECM-bound TGF-β is a suggested early response to dynamic compression causing a rapid increase of nuclear SMAD[20]. TGF-β canonically stimulates SMAD2/3 through the ALK5 receptor, however can shift stimulation towards SMAD1/5/9 phosphorylation through the ALK1 receptor[51]. It was however shown in bovine cartilage explants that excessive mechanical stress alone was not enough to cause this shift and increase SMAD1/5/9 activation[44]. Additionally, both physiological and excessive dynamic compression increased SMAD2/3 activation, which was not present in this study. It is suggested that TGF-β has a different effect in the presence or absence of PCM, which on day 5 after culture is still lacking[70]. Culturing the chondrocytes for a longer period to allow PCM production might thus influence TGF-β-SMAD signalling and will be discussed further in the next chapter. For later experiments, it was decided not to continue with hyperphysiological compression using 500 mbar, but instead use cytokines to induce a pathological condition. For this, IL-1β and TNF-α were used similar to literature [9, 71, 72].

A single mechanical stimulation session did not increase nuclear YAP. A lack of response could be caused by limited FA formation at day 5, as agarose does not allow cell-matrix interactions and limited ECM is formed as mentioned above. When more ECM is synthesised by the chondrocytes over time, more FAs could be formed that potentially influence YAP activity upon dynamic compression[25, 38, 39, 36]. Vinculin was visualised through immunofluorescence to detect FA formation in this study, which did not show a significant difference between static and compressed conditions with the used detection method[66]. The method was however formulated

for 2D applications, which may not work similarly on summed z-projections of 3D cell images. Another method used in literature is to analyse the change in cytoskeleton organisation by calculating an Edge Index[59]. This revealed that cytoskeleton remodelling upon dynamic compression was visible 1 minute after stimulation, but reverted back to a state similar to static condition 1 hour after stimulation[18]. Here the actin cytoskeleton showed a more spiked morphology upon compression compared to static conditions. In this thesis, fixation was done 1-2 hours after the last mechanical actuation session, which could explain the lack of difference between conditions. Although quantification of FAs was not possible, it is expected that sufficient ECM is produced when using longer culture times, as shown by[64]. To indicate regulation of YAP activation through FAs, different methods should be used to indicate FA formation in these 3D constructs, such as gene transcription of Rho/ROCK genes or proteins involved in FA formation.

In this study, it was chosen to estimate nuclear localization of proteins through immunofluorescence, due to the low sample availability and volume of experiments. A more quantitative method could be used such as Western Blot, separation of nuclear and cytoplasmic fraction or chromatin immunoprecipitation (ChIP). When using these methods however, the low sample size and contamination of agarose should still be taken into account and should therefore first be validated for the CoC platform.

Nuclear localization does not indicate gene expression, for which qPCR was used. The polysaccharide present in agarose can however cause contamination of the extracted RNA, which could explain the low absorption ratios seen in this study's results. It was also demonstrated that Trizol contamination causes incorrect measurements of RNA concentrations. Polysaccharides in agarose and cartilage tissues (GAG) can decrease RNA yield by co-purification in the phase-separation step of the Trizol extraction and inhibit reverse transcriptase[73]. This paper suggests that low temperatures of $0°C$ should be used when extracting with Trizol to reduce RNase activity. Additionally, phenol and guanidine isothiocyanate solutions (such as Trizol) and columns using a silica membrane can be useful for obtaining high-integrity RNA from cell/agarose constructs[74]. The RNeasy Microkit uses both techniques and showed the most reliable RNA extraction of the validated methods. Additionally, a limitation of low RNA quantities is that the nanodrop might not accurately measure the amount of extracted RNA. In the following experiments, four hydrogels were pooled for one sample and the whole sample after RNA extraction was used for cDNA synthesis. qPCR data was then normalised to the housekeeping gene RPS18 to compare gene transcription in different conditions. Lastly, agarase pre-treatment showed a small increase in purity, which could be explored in further studies to increase the purity.

Chapter 5

Protein activation upon compression

5.1 Results

To study the effect of dynamic compression on the activation of YAP and SMADs, two types of studies were performed. The first looks at the activation over time and the second one investigates the effect of dynamic compression in the presence of induced inflammation by the addition of cytokines. Additionally, matrix remodelling is assessed to be able to link these pathways to overall matrix production.

5.1.1 Influence of dynamic compression on cell behaviour over time

Immunofluorescence data shows no significant influence of dynamic compression on the nuclearisation of YAP and SMAD proteins, Figure 5.1 with statistical analysis in S2.9. The N/C ratio was studied over time by fixating samples on day 5, 9 and 12 of the mechanical actuation protocol. Only SMAD2/3 shows a difference between Static and Compression on day 5 and 9, but not day 12 (Figure 5.1A). Notably, on day 5 compression increases the N/C ratio compared to Static, while on day 9 compression decreases the N/C ratio. Additionally, a downward trend is seen for all proteins and conditions, except for SMAD2/3 where Static D9 shows a slight increase in the mean compared to D5. This suggests that the activity of all proteins decreases over time in this experimental setting, even with mechanical stimulation. For YAP and SMAD2/3, a larger decrease in N/C ratio is seen from day 9 to day 12 compared to the decrease from day 5 to day 9. SMAD1/5/9 shows the smallest decrease and no difference between conditions. All proteins show a N/C ratio of <1 at day 12, indicating that the proteins mainly reside in the cytoplasm. SMAD2/3 shows a higher N/C ratio compared to SMAD1/5/9, which is in line with the antagonistic nature of both pathways. Due to the limited amount of available samples, a small sample size was used per condition.

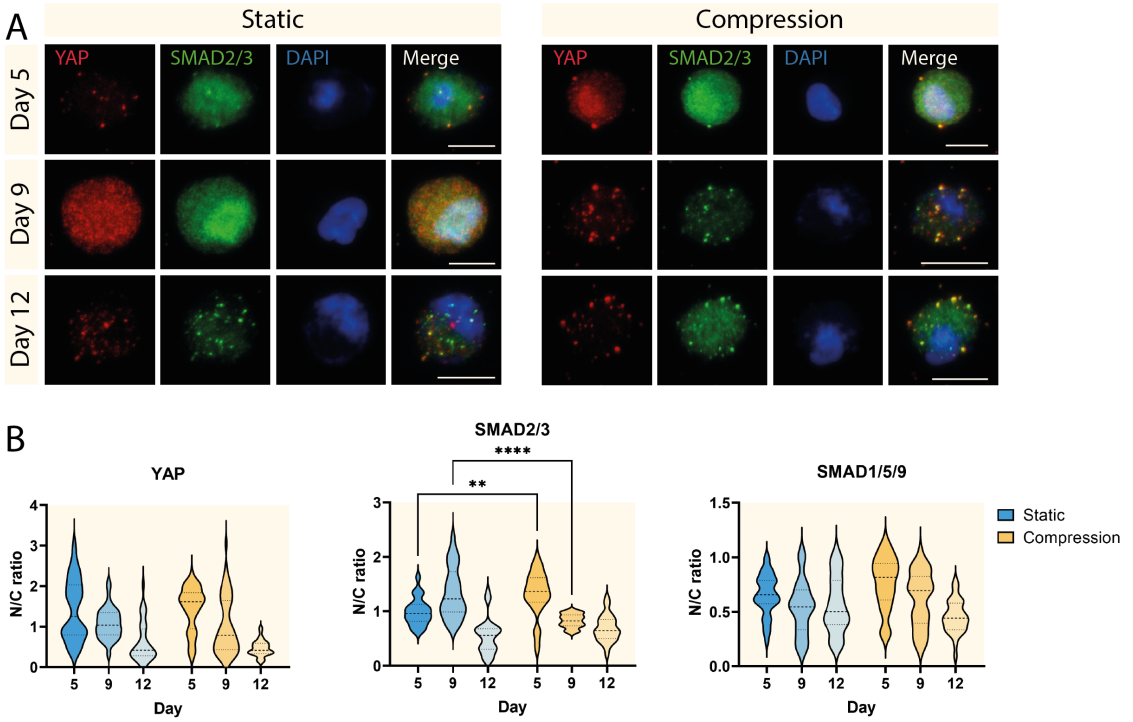

Figure (5.1) Influence of dynamic compression (300 mbar) compared to static condition over time in HPC. (A) Representative immunofluorescence images of YAP and SMAD2/3 ABs with DAPI, SMAD1/5/9 is not shown as there is little difference between conditions. Note that images are cropped in different sizes, but all scalebars represent 10 µM. (B) N/C ratio over time for YAP, SMAD2/3 and SMAD1/5/9 calculated from immunofluorescence images. N = 1 chip (SMADs) or 2 chips (YAP), 23-43 cells analysed per chip. Statistical analysis is represented in S2.9, Pvalues: $0.001 < P <= 0.01^{**}$, $P <= 0.0001^{****}$

Dynamic compression does not show beneficial ECM production according to GAG staining and immunofluorescence of aggrecan and collagen 2, Figure 5.2. For this experiment, samples previously used for immunofluorescence were re-used for Alcian Blue staining. A blue shell around the cells indicates formation of a PCM, which is visible in the static condition but less for the compressed condition. The mean gray value relative to a no cell control is shown in Figure 5.2B, which shows high variability in both conditions. In addition, no upward trend is detected as would be expected when looking at ECM production over time. Mechanical stimulation of chondrocytes has proven beneficial for matrix production in literature[21, 51, 64, 75], however these results show no clear benefit of dynamic compression. There are some cells surrounded by a PCM in each condition, though the number of cells presenting a PCM is larger in the static condition.

Figure 5.4C shows two situations that are found in the samples, one with and one without a PCM. When overexpressing the immunofluorescence images, aggrecan can be seen outside the cell indicating formation of PCM. Collagen 2 is less often found outside of the cell. An attempt was done to quantify the matrix deposition outside the cell, however due to the absence of a membrane marker this did not succeed. In static conditions there was generally more aggrecan detected outside the cell compared to compressed conditions.

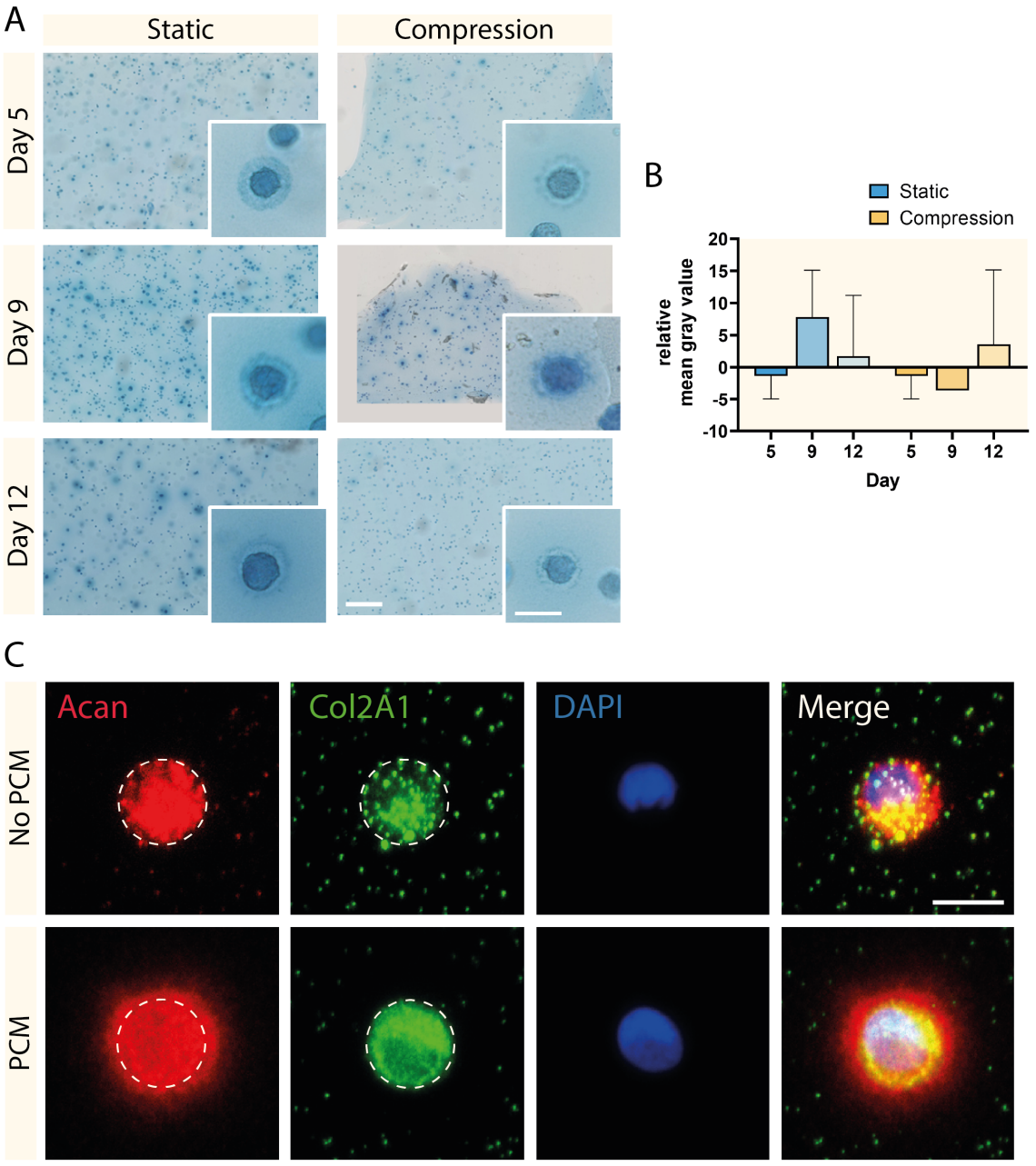

Figure (5.2) ECM production over time in static and compressed (300mbar) conditions in HPC (A) GAG production through Alcian Blue staining showing the hydrogel (scalebar = 200 µm) and zoomed in (scalebar = 20 µm), (B) Mean gray values relative to no cell control showing variability between days and conditions, N=3 chips. (C) Immunofluorescence images of matrix components in HPC Satic day 12, indicating ECM deposition when Acan shows outside the cell, indicated with a dashed circle. The brightness of the images is adjusted to show this effect. Scalebar = 10 µm, N=1 chip

5.1.2 Influence of pro-inflammatory cytokines on chondrocyte behaviour in response to dynamic compression

Dynamic compression does not affect YAP nuclearisation in pathological condition, Figure 5.3A and B. The results show increased YAP nuclearisation in chondrocytes when stimulated with cytokines, suggesting the influence of inflammation on YAP. However, no difference is seen when compression is applied. Downstream target gene CTGF- is upregulated upon compression, which suggests increased transcriptional activity of YAP, Figure 5.3D. Note that no statistical analysis was done for the PCR data as the data is represented as relative fold change to normal static condition.

Dynamic compression attenuates SMAD2/3 nuclearisation and stimulates SMAD1/5/9 activation in pathological conditions. Upon addition of cytokines, the N/C ratio is increased for SMAD2/3 while SMAD1/5/9 is not influenced, Figure 5.3A and B. In combination with dynamic compression, the N/C ratio increase of SMAD2/3 is less compared to static condition. Notable is the distribution here, which shows that this effect is more prominent in part of the chondrocytes in the sample. The opposite effect is seen for SMAD1/5/9, where cytokines alone do not influence nuclearisation but only in combination with dynamic compression. Measurements of TGF-β1 concentration in the medium show an initial increase after the first day of mechanical stimulation, Figure 5.3C. However on day 2 of mechanical stimulation, the TGF-β1 concentration returns to a similar value in all conditions, around 51 pg/mL. Cytokines thus do not affect this concentration.

Dynamic compression and inflammation show a role in YAP-SMAD2/3 transcription. CTGF-, Pai-1 and Id2 are downstream targets of YAP-TEAD, YAP-SMAD2/3 and YAP-SMAD1/5/9 transcription respectively. A change of transcriptional activity in these genes gives an estimation of the complex formed in the nucleus. CTGF- transcription is upregulated upon dynamic stimulation, suggesting YAP-TEAD complexion is stimulated upon compression, Figure 5.3D. Both CTGF- and Pai-1 are downregulated upon the addition of cytokines, suggesting an inhibitory role of inflammation on YAP-TEAD and YAP-SMAD2/3 complexing. In addition, Id2 is not affected by cytokines nor mechanical stimulation, suggesting no influence of the YAP-SMAD1/5/9 binding. Interestingly, inflammation downregulates transcription of CTGF- and Pai-1, but not of YAP itself.

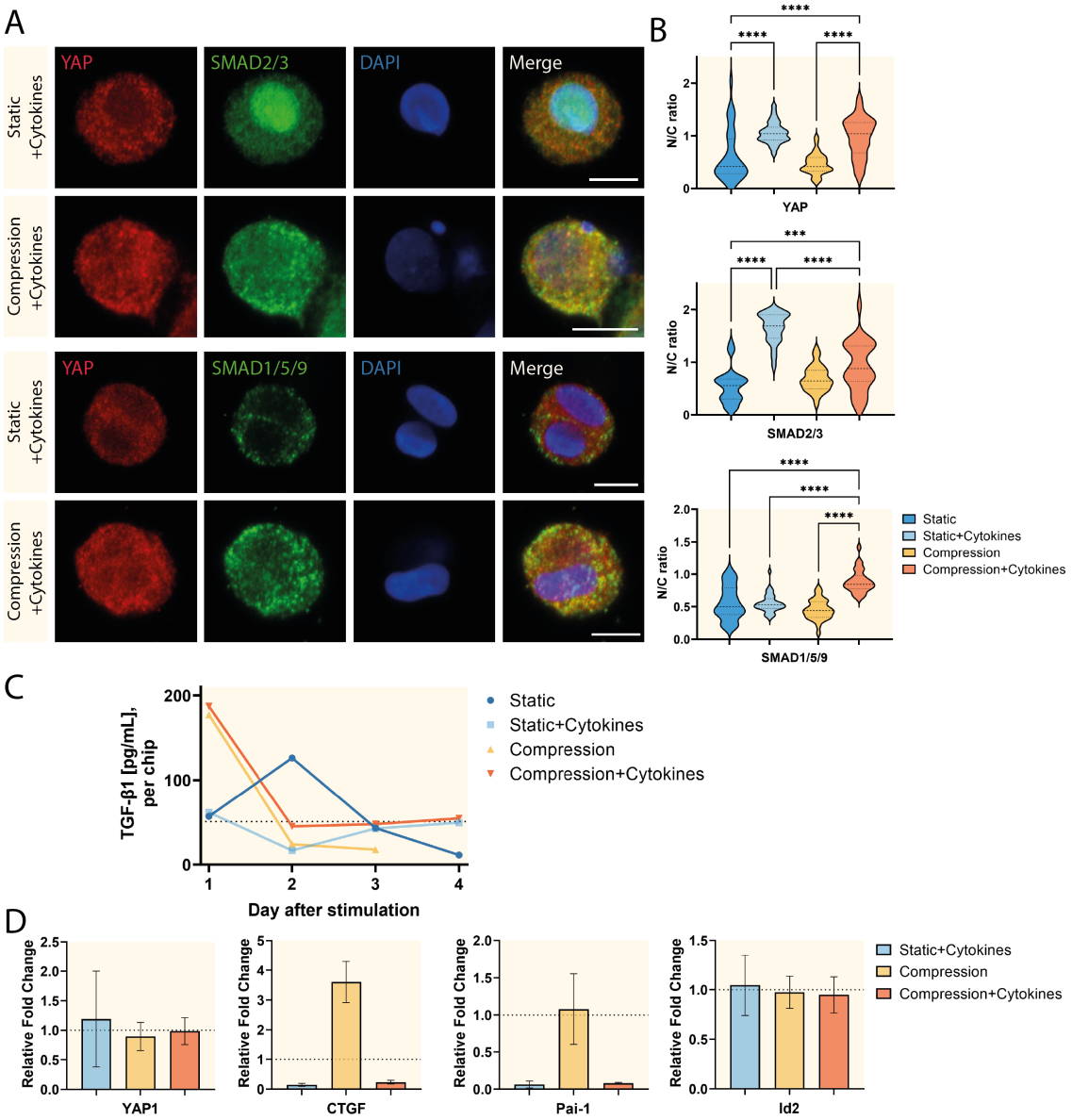

Figure (5.3) Influence of cytokines and dynamic compression (300 mbar) in HPC (A) Immunofluorescence images of single cells representative for each condition, scale bar = 10 µm. (B) N/C ratio of YAP, SMAD2/3 and SMAD1/5/9 detected from the immunofluorescence images, N=1 chip (SMADs) or N=2 chips (YAP), 26-40 cells analysed per chip. Data of normal condition is re-used for comparison. (C) TGF-β1 concentration measured with ELISA and normalised to DNA quantity. Shown is day 1-4 after mechanical stimulation, which corresponds to day 6-9 of the stimulation protocol, the full graph is shown in S2.11. Additionally the viability at day 12 is presented in S2.12 (D) RT-qPCR fold change of YAP1, CTGF-, Pai-1 and Id2 gene expression with respect to normal static condition and normalised to housekeeping gene RPS18, N=3 samples of 4 chips pooled, measured in duplo. Note the different scales of y-axes Pvalues: $0.0001 < P <= 0.001^{***}$, $P <= 0.0001^{****}$

Dynamic compression attenuates MMP13 activity in pathological condition. Addition of cytokines shows to reduce GAG production in static conditions, while some GAG shells can still be seen in compressed conditions, Figure 5.4A. As expected, RT-qPCR confirms the donwregulation of Acan and Col2A1 in pathological conditions, while matrix degrading enzymes MMP13 and ADAMTS5 are upregulated, Figure 5.4B. MMP13 is less upregulated when mechanically stimulating the pathological condition, suggesting a protective role of loading in cartilage degradation. Notably, both conditions with cytokines do not upregulate Collagen 10, which is a hypertrophy marker often used to indicate OA. This might be an effect developing later in OA. Immunofluorescence of Acan and Col2A1 indicates notable deposition of these ECM proteins upon addition of cytokines, Figure 5.4C. In addition, cells appear to be larger compared to the normal conditions shown in Figure 5.1A. Proliferation was also seen in pathological conditions which was not seen in normal conditions.

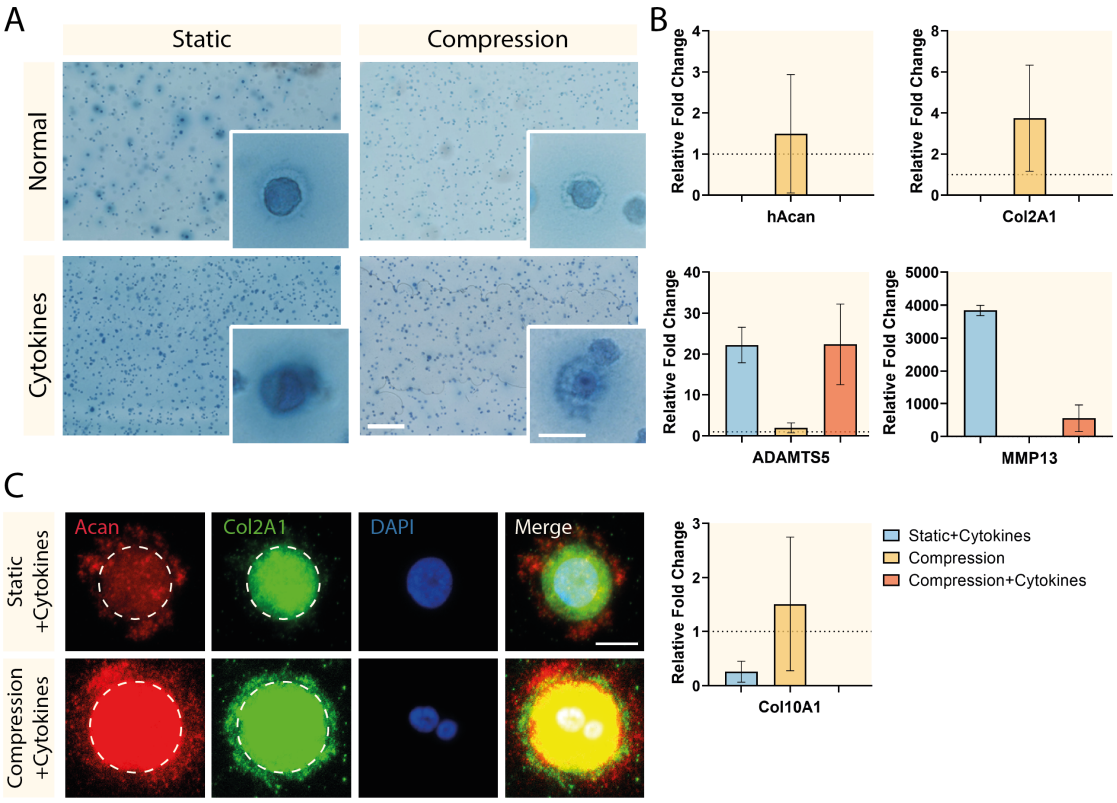

Figure (5.4) Influence of cytokines and compression (300 mbar) on the ECM production in HPC (A) GAG production through Alcian Blue staining showing the hydrogel (scalebar = 200 µm) and zoomed in (scalebar = 20 µm), a blue shell indicating PCM formation, N=3 chips. Data of normal condition is re-used for comparison. (B) RT-qPCR fold change of ECM components and degradation enzymes with respect to static normal condition and normalised to housekeeping gene RPS18, collagen X acts as hypertrophy marker, N=3 samples of 4 chips pooled, measured in duplo. Note the different scales of y-axes. (C) Immunofluorescence images of single cells showing matrix components. Acan outside of the cell (indicated with dashed line) indicates ECM deposition, the brightness of all images is adjusted to show this effect. Scalebar = 10 µm

5.2 Discussion

The aim of this thesis was to explore the inner workings of chondrocyte mechanobiology upon dynamic compression. It was decided to focus on YAP as this protein has shown the potential to attenuate cartilage degradation in OA[47, 57]. These papers however are inconsistent on whether upregulation or downregulation of YAP is beneficial as a potential treatment. The development of OA is linked to abnormal mechanical loading, while physiological loading of articular cartilage has shown beneficial to maintain cartilage homeostasis and preventing degradation in OA [76, 9, 69]. The suggested protective benefit of YAP could possibly be caused by interaction with pathways involved in matrix remodelling, which are influenced by mechanical loading. Previous studies on YAP activation in response to mechanical stimulation is limited to the effect of stiffness, cell area, and cell density. In this study, the effect of dynamic compression on YAP activation in chondrocytes was studied with and without induced inflammation.

The results of this study suggests that YAP nuclearisation is not influenced by dynamic compression. Upregulation of CTGF was however seen in upon compression, suggesting an increase of YAP-TEAD transcriptional activity. A regulatory role of FAs and actin stress fibers has previously been shown through Hippo-dependent and Hippo-independent pathways[25, 38, 35, 37]. Upon mechanical compression, the ECM deforms which propagates tensional and compressive forces on the cells, regulating cytoskeletal remodelling and stress fiber recruitment. It was therefore expected that, similar to increased FA and stress fiber formation in stiffer substrates, YAP activity would increase by mechanical compression. In the obtained results however, physiological compression of 300 mbar was not beneficial for GAG production, causing less FA formation and stress fiber recruitment. Nonetheless, a decreasing trend in N/C ratio of YAP was seen in both static and compressed conditions, suggesting no influence of the applied stimuli. Because agarose does not allow cell adhesion, the stiffness of this matrix was not expected to influence YAP nuclearisation.

YAP activity has also been linked to increased cytokine concentrations[47, 57]. It was reported previously that IL-6, IL-1β and TNF-α concentrations increase upon seeding of chondrocytes in the CoC platform, suggesting a 7 day static culture period to reduce the influence of these cytokines[64]. In this thesis, a static culture period of 5 days was used to shorten the experimental protocol and because IL-1β and TNF-α showed enough reduction at this time point. Upon addition of IL-1β and TNF-α in the pathological condition, an increase in nuclear YAP was presented. The starting N/C ratio of YAP at day 5 could therefore be linked to this initial increase of cytokines upon seeding and the decrease of N/C ratio related to the reduction of cytokine concentration over time. In future experiments, it would thus be beneficial to use a longer static culture period before evaluating protein nuclearisation (7-12 days), to reduce this effect of cytokines after seeding and ensure sufficient ECM production as mentioned above. Performing mechanical actuation experiments without the effect of cytokines and with a physiologically relevant ECM will give more information about the influence of dynamic compression on YAP activity.

In this study, physiological compression does not show an increase in TGF-β/SMAD activation, in contrast to literature[44]. This increase has been suggested to originate from release of latent TGF-β bound to the ECM, which can be released through compression. However, TGF-β-SMAD2/3 activity is dependent on duration

of the stimulation[20] and presence of an established PCM[70]. The absence of a response in SMAD2/3 nuclearisation upon stimulation could therefore be explained by the lack of ECM production in this thesis. In contrast, SMAD1/5/9 was not expected to be activated through mechanical stimulation. Even excessive mechanical stress alone was not enough to cause a shift toward SMAD1/5/9 pathway [44], which is in line with the obtained results.

Next to the lack of ECM production, some other limitations should be taken into account. One is the use of only one donor for all mechanical actuation experiments. The obtained results are therefore not representative of the studied biological phenomena, but can be seen as a proof of concept for studying mechanobiology in this platform. To make significant conclusions on the role of dynamic mechanical compression on the activation of YAP, these experiments should be repeated using several donors to increase the biological sample size. Additionally, there was variability in ECM production between samples, inconsistent with previous studies that showed increased ECM production upon compression[58, 64, 51]. A potential cause is the seeding quality of the gel, which can be improved by experience of handling the platform. However, this does not account for the variability in the static conditions. An additional method to enhance matrix production is mixing agarose with collagen I[77]. This could provide a better microenvironment to regulate the forces felt by the chondrocytes upon mechanical compression, and reduce the culturing time for achieving sufficient ECM production. Lastly, the period between mechanical stimulation and fixation of the samples might cause loss of data. Similar experiments showed that cytoskeleton remodelling upon mechanical compression was visible when directly fixating the samples after stimulation, which was reverted after on hour [18].

Furthermore, the obtained results suggest that dynamic compression in pathological conditions does not affect YAP nuclearisation, but instead affects binding to different transcription factors. In this case, CTGF- and Pai-1 were downregulated upon addition of cytokines. CTGF- is a downstream target of YAP-TEAD interactions, but also of YAP-SMAD2/3[78], which has shown downregulation in mice upon TNF-α treatment [79]. Additionally, Pai-1 expression is influenced by cytokines, suggesting inhibition of gene transcription by the YAP-SMAD2/3 complex. Downregulation of both these genes could thus be an effect of inflammation on YAP-SMAD2/3 interaction. YAP overexpression can inhibit hypertrophy [79], similar to the role of SMAD2/3 in chondrocyte maturation, which highlights this relation.

Additionally, inflammatory cytokines were shown to activate Hippo signalling to promote YAP sequestering in HEK cells, however not in chondrocytes[47]. This is in line with the increased nuclearisation of YAP upon the addition of cytokines in the results. Upregulation of YAP was connected to induced OA in mice[57], however no upregulation of YAP transcription was shown in this study. Furthermore, an increased cell size was seen in pathological conditions, which has been reported to increase YAP nuclearisation independent of FA formation[40]. The increase of N/C ratio in this thesis could therefore also be caused by the increased cell size. The results also revealed that MMP13 upregulation by cytokines was attenuated by physiological loading, suggesting some benefit of dynamic compression in protecting cartilage degeneration. In this situation, nuclear YAP was also increased. Future research could investigate if the increase of nuclear YAP is related to the attenuation of MMP13 upregulation, by inhibiting or overexpressing YAP through inhibitors/stimulators. Multiple interactions of YAP and the Hippo pathway with

Nf-κB signalling have been identified in literature[80]. The experimental set-up in this thesis was however not enough to give insight into the potential role of YAP in Nf-κB signalling.

Finally, mechanical stimulation in the pathological condition was able to increase nuclear SMAD1/5/9. This is in line with earlier research that showed that mechanical stimulation in combination with cytokines can induce a shift in TGF-β signalling towards SMAD1/5/9 [44]. No upregulation of Id2 was shown, a target downstream of YAP-SMAD1/5/9, suggesting that YAP-SMAD1/5/9 interaction is not promoted in this condition, even though nuclear SMAD1/5/9 was increased. TGF-β stimulation of chondrocytes has demonstrated upregulation of Id1, which was used to indicate a shift of SMAD pathways by looking at the Id1/Pai-1 ratio (indicating SMAD1/5/9 / SMAD2/3 ratio)[51]. Therefore, multiple downstream targets of transcription complexes should be used instead of a single target in future research, to provide a better indication of the transcription activity. Due to limited RNA content in this study, only a few selected genes were included to indicate each interaction.

Chapter 6

Conclusion & Future Outlook

In this thesis, YAP/TAZ (YAP) activity was analysed upon mechanical dynamic compression in chondrocytes. The influence of compression was investigated using a Cartilage-on-Chip (CoC) platform to provide mechanical stimulation.

First, analysis methods were validated for the CoC platform and parameters analysed for mechanical stimulation. Trizol extraction of RNA demonstrated high contamination in concentration and purity measurements. In the end, column based extraction with a silica membrane presented the least contamination. In addition, a small increase in purity was obtained when using agarase pre-treatment, which could be explored in future research. Analysis of vinculin did not show a difference in Focal Adhesion (FA) assembly when stimulated with 300 and 500 mbar compression. To study the influence of compression on cytoskeleton remodelling and FA assembly, a different method should be explored and the samples should be fixed immediately after mechanical stimulation. Furthermore, a high variability in gel displacement between chips was detected likely due to the seeding quality, which should be taken care of in future experiments.

The results indicate that YAP nuclearisation is not influenced by mechanical physiological compression in both normal and pathological conditions. Compression might instead play a role in the binding of YAP with other transcription factors. Additionally, it was shown that inflammation increases nuclear SMAD2/3, which is attenuated by physiological compression. In contrast, compression in the pathological condition induced SMAD1/5/9 activation. Furthermore, an increased cell size was noted in pathological conditions, which could also increase YAP nuclearisation. Upregulation of MMP13 was attenuated when compression was applied in pathological conditions, indicating a protective role of dynamic loading on cartilage degradation.

The objectives of this thesis were to investigate the influence of dynamic compression on YAP activation in a normal and pathological condition in chondrocytes. From the results can be concluded that nuclearisation of YAP is increased upon inflammation but not upon dynamic compression. This is in contrast to the hypothesis that dynamic compression increases nuclear YAP similar to incresaed substrate stiffness. Compression might instead influence binding of YAP to other transcription factors, where dynamic compression increases YAP-TEAD binding while inflammation decreases YAP-SMAD2/3 binding. Furthermore, attenuation of MMP13 upregulation upon inflammation might be related to increased nuclear YAP, which should be explored further.

By unraveling the role of YAP in cartilage homeostasis, their benefit as thera-

peutic intervention for osteoarthritis (OA) could be discovered. YAP has demonstrated to attenuate cartilage degradation in OA, but there is controversy regarding the route of action. Additionally, activation of this pathway shows a high dependency on the type of tissue. Organ-on-Chip technology provides a platform to study mechanobiology in specific tissues, without influence of other tissues. This type of research can provide new insights into the initiation and progression of cartilage degradation. By studying different mechanotransduction pathways on chip, new strategies to mediate OA could be found and tested.

Some limitations of this study are the limited biological sample size used and the variability in Extracellular Matrix (ECM) production in the samples to simulate the native microenvironment. In future research, several cell donors should be used to increase the biological relevance of the results. To study the influence of mechanical compression on mechanotransduction pathways, a pre-culture period should be used to ensure sufficient production of ECM in both static and compressed conditions. Additionally, several downstream targets of transcription should be used to validate transcriptional co-activity. Furthermore, different methods could be explored to analyse pathway activation, taking into account the low sample size and possible contamination of agarose.

This thesis was focused on the activation of YAP upon dynamic compression. To further explore their role in cartilage remodelling, YAP inhibitors and stimulators could be used to relate YAP activity to cartilage development by looking at ECM production over time in the agarose hydrogel. By first pre-culturing the chondrocytes to obtain a more physiological relevant PCM, inihbitors and stimulators could be used to uncover their role in matrix homeostasis. By combining this with mechanical compression and cytokines, more insight into the physiological maintenance of cartilage and disease could be gained. Additionally, this research could be reproduced to investigate other mechanotransduction pathways such as Ca2+ signalling, primary cilia and other biochemical signalling pathways.

Acknowledgements

I would like to express my sincere gratitude to my daily supervisor, dr. Nuno Araújo da Cunha Gomes, for their invaluable guidance and support throughout my Master Thesis. Your patience and enthusiasm for teaching me in the lab and providing feedback helped me have a great time during my thesis. You were always ready to help me during my nearly daily round of questions and always very enthusiastic about helping me put my ideas to work. Even if it was often too early in the morning, a coffee was needed or the weekend couldn't come soon enough, problems were often solved together.

In addition, many thanks go out to dr. Liliana Moreira Teixeira Leijten for guiding me during this process. Your weekly supervision helped me look beyond only performing experiments and think critically about the research process. Their expertise, patience, and encouragement have been instrumental in helping me navigate the challenges of academic research and in shaping my academic and professional development.

I would also like to extend my appreciation to the other members of the examination committee for their time and expertise in evaluating my thesis. Thank Marcel Karperien for giving me the opportunity to work in his group and make me realise that research is only as good as your controls. Thanks to Jeroen Rouwkema for being my external member. Their insights and constructive feedback have been invaluable in helping me to improve my work and to better understand the subject matter.

A special thanks go out to Laurens Spoelstra for their assistance in helping me understand and use the platform. Even as a fellow master student working on your thesis, your patience and guidance have been invaluable in ensuring that I was able to effectively utilise the platform and complete my work. Even when you had no time and outside of office hours you were quick to reply or research my questions which helped me succeed my thesis.

Lastly, I would like to thank the members of the DBE group for advising me in the lab, helping me with analysing data and in general providing a comfortable work environment. A special thanks to Jacqueline Plass and Irene Konings for helping me acquire the space and materials needed for my large experiments, Tom Knop for taking the time to help me obtain amazing Zeiss Confocal images and all Actuation People for sharing expertise on the platform. Also thank all the students at the student table for offering support during both the up and down moments in research and making this master project a fun experience.

Bibliography

[1] J. M. Oomen, Y. A. Peters, C. H. van den Ende, H. J. Schers, W. J. Assendelft, J. E. Vriezekolk, and S. Koëter, "Quality of knee osteoarthritis care in the Netherlands: a survey on the perspective of people with osteoarthritis," *BMC Health Services Research*, vol. 22, 12 2022.

[2] A. Voor Programma, Z. Zorg, and P. E. D. Eysink, "Epidemiologische data van ziekten van het botspierstelsel en bindweefsel,"

[3] "OARSI White Paper - Osteoarthritis: A Serious Disease," tech. rep., Osteoarthritis Research Society International, 12 2016.

[4] M. Kloppenburg and F. Berenbaum, "Osteoarthritis year in review 2019: epidemiology and therapy," *Osteoarthritis and Cartilage*, vol. 28, pp. 242–248, 3 2020.

[5] R. Dreier, "Hypertrophic differentiation of chondrocytes in osteoarthritis: The developmental aspect of degenerative joint disorders," *Arthritis Research and Therapy*, vol. 12, pp. 1–11, 9 2010.

[6] D. Chen, J. Shen, W. Zhao, T. Wang, L. Han, J. L. Hamilton, and H. J. Im, "Osteoarthritis: toward a comprehensive understanding of pathological mechanism," *Bone research*, vol. 5, 1 2017.

[7] D. J. Leong, J. A. Hardin, N. J. Cobelli, and H. B. Sun, "Mechanotransduction and cartilage integrity," *Annals of the New York Academy of Sciences*, vol. 1240, pp. 32–37, 12 2011.

[8] S. Glyn-Jones, A. J. Palmer, R. Agricola, A. J. Price, T. L. Vincent, H. Weinans, and A. J. Carr, "Osteoarthritis," *The Lancet*, vol. 386, pp. 376–387, 7 2015.

[9] M. B. Goldring and K. B. Marcu, "Cartilage homeostasis in health and rheumatic diseases," *Arthritis Research and Therapy*, vol. 11, pp. 1–16, 5 2009.

[10] A. J. Sophia Fox, A. Bedi, and S. A. Rodeo, "The basic science of articular cartilage: Structure, composition, and function," *Sports Health*, vol. 1, pp. 461–468, 11 2009.

[11] H. K. Gahunia, A. E. Gross, K. P. Pritzker, P. S. Babyn, and L. Murnaghan, "Articular cartilage of the knee: Health, disease and therapy," *Articular Cartilage of the Knee: Health, Disease and Therapy*, pp. 1–498, 1 2020.

[12] T. Hodgkinson, D. C. Kelly, C. M. Curtin, and F. J. O'Brien, "Mechanosignalling in cartilage: an emerging target for the treatment of osteoarthritis," *Nature Reviews Rheumatology 2021 18:2*, vol. 18, pp. 67–84, 12 2021.

[13] I. Kutzner, B. Heinlein, F. Graichen, A. Bender, A. Rohlmann, A. Halder, A. Beier, and G. Bergmann, "Loading of the knee joint during activities of daily living measured in vivo in five subjects," *Journal of biomechanics*, vol. 43, pp. 2164–2173, 8 2010.

[14] S. P. Messier, D. J. Gutekunst, C. Davis, and P. DeVita, "Weight loss reduces knee-joint loads in overweight and obese older adults with knee osteoarthritis," *Arthritis and rheumatism*, vol. 52, pp. 2026–2032, 7 2005.

[15] B. D. Elder and K. A. Athanasiou, "Hydrostatic pressure in articular cartilage tissue engineering: from chondrocytes to tissue regeneration," *Tissue engineering. Part B, Reviews*, vol. 15, pp. 43–53, 3 2009.

[16] C. Chen, D. T. Tambe, L. Deng, and L. Yang, "Biomechanical properties and mechanobiology of the articular chondrocyte," *American Journal of Physiology - Cell Physiology*, vol. 305, pp. 1202–1208, 12 2013.

[17] Z. Lin, C. Willers, J. Xu, and M. H. Zheng, "The chondrocyte: biology and clinical application," *Tissue engineering*, vol. 12, pp. 1971–1984, 7 2006.

[18] M. M. Knight, T. Toyoda, D. A. Lee, and D. L. Bader, "Mechanical compression and hydrostatic pressure induce reversible changes in actin cytoskeletal organisation in chondrocytes in agarose," *Journal of Biomechanics*, vol. 39, pp. 1547–1551, 1 2006.

[19] T. Ikenoue, M. C. Trindade, M. S. Lee, E. Y. Lin, D. J. Schurman, S. B. Goodman, and R. L. Smith, "Mechanoregulation of human articular chondrocyte aggrecan and type II collagen expression by intermittent hydrostatic pressure in vitro," *Journal of Orthopaedic Research*, vol. 21, no. 1, pp. 110–116, 2003.

[20] C. Bougault, E. Aubert-Foucher, A. Paumier, E. Perrier-Groult, L. Huot, D. Hot, M. Duterque-Coquillaud, and F. Mallein-Gerin, "Dynamic Compression of Chondrocyte-Agarose Constructs Reveals New Candidate Mechanosensitive Genes," *PLOS ONE*, vol. 7, p. e36964, 5 2012.

[21] M. A. Brady, S. D. Waldman, and C. R. Ethier, "The Application of Multiple Biophysical Cues to Engineer Functional Neocartilage for Treatment of Osteoarthritis. Part II: Signal Transduction," *https://home.liebertpub.com/teb*, vol. 21, pp. 20–33, 10 2014.

[22] S. J. Gilbert and E. J. Blain, "Cartilage mechanobiology: How chondrocytes respond to mechanical load," *Mechanobiology in Health and Disease*, pp. 99–126, 1 2018.

[23] C. A. Paggi, B. Venzac, M. Karperien, J. C. Leijten, and S. Le Gac, "Monolithic microfluidic platform for exerting gradients of compression on cell-laden hydrogels, and application to a model of the articular cartilage," *Sensors and Actuators B: Chemical*, vol. 315, p. 127917, 7 2020.

[24] Z. Zhao, Y. Li, M. Wang, S. Zhao, Z. Zhao, and J. Fang, "Mechanotransduction pathways in the regulation of cartilage chondrocyte homoeostasis," *Journal of Cellular and Molecular Medicine*, vol. 24, pp. 5408–5419, 5 2020.

[25] F. Martino, A. R. Perestrelo, V. Vinarský, S. Pagliari, and G. Forte, "Cellular mechanotransduction: From tension to function," *Frontiers in Physiology*, vol. 9, p. 824, 7 2018.

[26] C. da Silva Madaleno, J. Jatzlau, and P. Knaus, "BMP signalling in a mechanical context – Implications for bone biology," *Bone*, vol. 137, p. 115416, 8 2020.

[27] M. M. Holledge, S. J. Millward-Sadler, G. Nuki, and D. M. Salter, "Mechanical regulation of proteoglycan synthesis in normal and osteoarthritic human articular chondrocytes – roles for $\alpha 5$ and $\alpha V\beta 5$ integrins," *Biorheology*, vol. 45, pp. 275–288, 1 2008.

[28] B. Pingguan-Murphy, M. El-Azzeh, D. L. Bader, and M. M. Knight, "Cyclic compression of chondrocytes modulates a purinergic calcium signalling pathway in a strain rate- and frequency-dependent manner," *Journal of cellular physiology*, vol. 209, pp. 389–397, 11 2006.

[29] F. Guilak, R. A. Zell, G. R. Erickson, D. A. Grande, C. T. Rubin, K. J. McLeod, and H. J. Donahue, "Mechanically induced calcium waves in articular chondrocytes are inhibited by gadolinium and amiloride," *Journal of orthopaedic research : official publication of the Orthopaedic Research Society*, vol. 17, no. 3, pp. 421–429, 1999.

[30] R. Ruhlen and K. Marberry, "The chondrocyte primary cilium," *Osteoarthritis and cartilage*, vol. 22, no. 8, pp. 1071–1076, 2014.

[31] A. K. T. Wann, N. Zuo, C. J. Haycraft, C. G. Jensen, C. A. Poole, S. R. McGlashan, and M. M. Knight, "Primary cilia mediate mechanotransduction through control of ATP-induced Ca2+ signaling in compressed chondrocytes," *FASEB journal : official publication of the Federation of American Societies for Experimental Biology*, vol. 26, pp. 1663–1671, 4 2012.

[32] M. A. Brady, S. D. Waldman, and C. R. Ethier, "The application of multiple biophysical cues to engineer functional neocartilage for treatment of osteoarthritis. Part II: Signal transduction," *Tissue Engineering - Part B: Reviews*, vol. 21, pp. 20–33, 2 2015.

[33] N. G. Thielen, P. M. van der Kraan, and A. P. van Caam, "TGFβ/BMP Signaling Pathway in Cartilage Homeostasis," *Cells 2019, Vol. 8, Page 969*, vol. 8, p. 969, 8 2019.

[34] M. K. Kim, J. W. Jang, and S. C. Bae, "DNA binding partners of YAP/TAZ," *BMB Reports*, vol. 51, no. 3, p. 126, 2018.

[35] O. Dobrokhotov, M. Samsonov, M. Sokabe, and H. Hirata, "Mechanoregulation and pathology of YAP/TAZ via Hippo and non-Hippo mechanisms," *Clinical and Translational Medicine*, vol. 7, p. e23, 12 2018.

[36] S. Dupont, L. Morsut, M. Aragona, E. Enzo, S. Giulitti, M. Cordenonsi, F. Zanconato, J. Le Digabel, M. Forcato, S. Bicciato, N. Elvassore, and S. Piccolo, "Role of YAP/TAZ in mechanotransduction," *Nature*, vol. 474, pp. 179–184, 6 2011.

[37] X. Cai, K. C. Wang, and Z. Meng, "Mechanoregulation of YAP and TAZ in Cellular Homeostasis and Disease Progression," *Frontiers in Cell and Developmental Biology*, vol. 9, p. 1333, 5 2021.

[38] M. Zarka, E. Haÿ, and M. Cohen-Solal, "YAP/TAZ in Bone and Cartilage Biology," *Frontiers in Cell and Developmental Biology*, vol. 9, 1 2021.

[39] D. Lachowski, E. Cortes, B. Robinson, A. Rice, K. Rombouts, A. E. Del Río Hernández, D. Lachowski, E. Robinson, B. Rice, A. Rombouts, and D. Río Hernández, "FAK controls the mechanical activation of YAP, a transcriptional regulator required for durotaxis," *The FASEB Journal*, vol. 32, pp. 1099–1107, 2 2018.

[40] G. Nardone, J. Oliver-De La Cruz, J. Vrbsky, C. Martini, J. Pribyl, P. Skládal, M. Pešl, G. Caluori, S. Pagliari, F. Martino, Z. Maceckova, M. Hajduch, A. Sanz-Garcia, N. M. Pugno, G. B. Stokin, and G. Forte, "YAP regulates cell mechanics by controlling focal adhesion assembly," *Nature Communications 2017 8:1*, vol. 8, pp. 1–13, 5 2017.

[41] M. Haroon, H. E. Boers, A. D. Bakker, N. G. Bloks, W. M. Hoogaars, L. Giordani, R. J. Musters, L. Deldicque, K. Koppo, F. L. Grand, J. Klein-Nulend, and R. T. Jaspers, "Reduced growth rate of aged muscle stem cells is associated with impaired mechanosensitivity," *Aging*, vol. 14, pp. 28–53, 1 2022.

[42] C. H. Heldin, K. Miyazono, and P. Ten Dijke, "TGF-beta signalling from cell membrane to nucleus through SMAD proteins," *Nature*, vol. 390, pp. 465–471, 12 1997.

[43] Y. Li and L. Xu, "Advances in understanding cartilage remodeling," *F1000Research*, vol. 4, 8 2015.

[44] W. Madej, A. van Caam, E. N. Blaney Davidson, P. M. van der Kraan, and P. Buma, "Physiological and excessive mechanical compression of articular cartilage activates Smad2/3P signaling," *Osteoarthritis and Cartilage*, vol. 22, pp. 1018–1025, 7 2014.

[45] M. Wu, B. Schölkopf, and G. Bakir, "Analysis of the mechanical behavior of chondrocytes in unconfined compression tests for cyclic loading," *Journal of biomechanics*, vol. 39, pp. 603–624, 4 2006.

[46] X. Houard, M. B. Goldring, and F. Berenbaum, "Homeostatic mechanisms in articular cartilage and role of inflammation in osteoarthritis," *Current rheumatology reports*, vol. 15, 11 2013.

[47] Y. Deng, J. Lu, W. Li, A. Wu, X. Zhang, W. Tong, K. K. Ho, L. Qin, H. Song, and K. K. Mak, "Reciprocal inhibition of YAP/TAZ and NF-κB regulates osteoarthritic cartilage degradation," *Nature Communications 2018 9:1*, vol. 9, pp. 1–14, 11 2018.

[48] K. B. Marcu, M. Otero, E. Olivotto, R. M. Borzi, and M. B. Goldring, "NF-κB Signaling: Multiple angles to target OA," *Current drug targets*, vol. 11, p. 599, 3 2010.

[49] M. C. Choi, J. Jo, J. Park, H. K. Kang, and Y. Park, "NF-κB Signaling Pathways in Osteoarthritic Cartilage Destruction," *Cells*, vol. 8, 7 2019.

[50] S. Rigoglou and A. G. Papavassiliou, "The NF-κB signalling pathway in osteoarthritis," *The International Journal of Biochemistry & Cell Biology*, vol. 45, pp. 2580–2584, 11 2013.

[51] T. Davisson, S. Kunig, A. Chen, R. Sah, and A. Ratcliffe, "Static and dynamic compression modulate matrix metabolism in tissue engineered cartilage," *Journal of Orthopaedic Research*, vol. 20, pp. 842–848, 7 2002.

[52] H. K. Vanyai, F. Prin, O. Guillermin, B. Marzook, S. Boeing, A. Howson, R. E. Saunders, T. Snoeks, M. Howell, T. J. Mohun, and B. Thompson, "Control of skeletal morphogenesis by the Hippo-YAP/TAZ pathway," *Development (Cambridge)*, vol. 147, 11 2020.

[53] X. Varelas, P. Samavarchi-Tehrani, M. Narimatsu, A. Weiss, K. Cockburn, B. G. Larsen, J. Rossant, and J. L. Wrana, "The Crumbs complex couples cell density sensing to Hippo-dependent control of the TGF-β-SMAD pathway," *Developmental cell*, vol. 19, pp. 831–844, 12 2010.

[54] Y. Li, I. Golshirazian, B. Asbury, J. Kim, and L. Xu, "Induction of high temperature requirement A1, a serine protease, by TGF-beta1 in knee joints of mouse models of OA," *Osteoarthritis and Cartilage*, vol. 20, pp. S143–S144, 4 2012.

[55] C. D. Kegelman, J. C. Coulombe, K. M. Jordan, D. J. Horan, L. Qin, A. G. Robling, V. L. Ferguson, T. M. Bellido, and J. D. Boerckel, "YAP and TAZ mediate osteocyte perilacunar/canalicular remodeling," *Journal of bone and mineral research : the official journal of the American Society for Bone and Mineral Research*, vol. 35, p. 196, 1 2020.

[56] Q. Wei, A. Holle, J. Li, F. Posa, F. Biagioni, O. Croci, A. S. Benk, J. Young, F. Noureddine, J. Deng, M. Zhang, G. J. Inman, J. P. Spatz, S. Campaner, and E. A. Cavalcanti-Adam, "BMP-2 Signaling and Mechanotransduction Synergize to Drive Osteogenic Differentiation via YAP/TAZ," *Advanced Science*, vol. 7, p. 1902931, 8 2020.

[57] Y. Gong, S. J. Li, R. Liu, J. F. Zhan, C. Tan, Y. F. Fang, Y. Chen, and B. Yu, "Inhibition of YAP with siRNA prevents cartilage degradation and ameliorates osteoarthritis development," *Journal of Molecular Medicine*, vol. 97, pp. 103–114, 1 2019.

[58] M. D. Buschmann, Y. A. Gluzband, A. J. Grodzinsky, and E. B. Hunziker, "Mechanical compression modulates matrix biosynthesis in chondrocyte/agarose culture," *Journal of Cell Science*, vol. 108, pp. 1497–1508, 4 1995.

[59] M. M. Knight, B. D. Idowu, D. A. Lee, and D. L. Bader, "Temporal changes in cytoskeletal organisation within isolated chondrocytes quantified using a novel image analysis technique," *Medical and Biological Engineering and Computing 2001 39:3*, vol. 39, no. 3, pp. 397–404, 2001.

[60] D. A. Lee, M. M. Knight, J. F. Bolton, B. D. Idowu, M. V. Kayser, and D. L. Bader, "Chondrocyte deformation within compressed agarose constructs at the cellular and sub-cellular levels," *Journal of Biomechanics*, vol. 33, pp. 81–95, 1 2000.

[61] D. Huh, B. D. Matthews, A. Mammoto, M. Montoya-Zavala, H. Yuan Hsin, and D. E. Ingber, "Reconstituting organ-level lung functions on a chip," *Science*, vol. 328, pp. 1662–1668, 6 2010.

[62] P. Occhetta, A. Mainardi, E. Votta, Q. Vallmajo-Martin, M. Ehrbar, I. Martin, A. Barbero, and M. Rasponi, "Hyperphysiological compression of articular cartilage induces an osteoarthritic phenotype in a cartilage-on-a-chip model," *Nature Biomedical Engineering 2019 3:7*, vol. 3, pp. 545–557, 6 2019.

[63] Q. Zhang, X. Fang, W. Zhao, and Q. Liang, "The transcriptional coactivator YAP1 is overexpressed in osteoarthritis and promotes its progression by interacting with Beclin-1," *Gene*, vol. 689, pp. 210–219, 3 2019.

[64] C. A. Paggi, J. Hendriks, M. Karperien, and S. L. Gac, "Emulating the chondrocyte microenvironment using multi-directional mechanical stimulation in a cartilage-on-chip," *Lab on a Chip*, 2022.

[65] C. I. Johnson, D. J. Argyle, and D. N. Clements, "In vitro models for the study of osteoarthritis," *The Veterinary Journal*, vol. 209, pp. 40–49, 3 2016.

[66] U. Horzum, B. Ozdil, and D. Pesen-Okvur, "Step-by-step quantitative analysis of focal adhesions," *MethodsX*, vol. 1, no. 1, pp. 56–59, 2014.

[67] D. J. Barry, C. Gerri, D. M. Bell, R. D'Antuono, and K. K. Niakan, "GIANI: open-source software for automated analysis of 3D microscopy images," *Journal of Cell Science*, vol. 135, 5 2022.

[68] C. L. Chiu, J. S. Aguilar, C. Y. Tsai, G. K. Wu, E. Gratton, and M. A. Digman, "Nanoimaging of Focal Adhesion Dynamics in 3D," *PLOS ONE*, vol. 9, p. e99896, 6 2014.

[69] P. Dolzani, E. Assirelli, L. Pulsatelli, R. Meliconi, E. Mariani, and S. Neri, "Ex vivo physiological compression of human osteoarthritis cartilage modulates cellular and matrix components," *PLoS ONE*, vol. 14, 9 2019.

[70] G. J. Van Osch, S. W. Van Der Veen, P. Bumat, and H. L. Verwoerd-Verhoef, "Effect of transforming growth factor-β on proteoglycan synthesis by chondrocytes in relation to differentiation stage and the presence of pericellular matrix," *Matrix Biology*, vol. 17, no. 6, pp. 413–424, 1998.

[71] M. B. Goldring, "Osteoarthritis and cartilage: the role of cytokines," *Current rheumatology reports*, vol. 2, no. 6, pp. 459–465, 2000.

[72] L. Sun, X. Wang, and D. L. Kaplan, "A 3D cartilage - inflammatory cell culture system for the modeling of human osteoarthritis," *Biomaterials*, vol. 32, p. 5581, 8 2011.

[73] J. C. Groppe and D. E. Morse, "Isolation of full-length RNA templates for reverse transcription from tissues rich in RNase and proteoglycans," *Analytical biochemistry*, vol. 210, no. 2, pp. 337–343, 1993.

[74] T. Ogura, A. Tsuchiya, T. Minas, and S. Mizuno, "Methods of high integrity RNA extraction from cell/agarose construct," *BMC Research Notes*, vol. 8, p. 644, 11 2015.

[75] M. Jin, E. H. Frank, T. M. Quinn, E. B. Hunziker, and A. J. Grodzinsky, "Tissue Shear Deformation Stimulates Proteoglycan and Protein Biosynthesis in Bovine Cartilage Explants," *Archives of Biochemistry and Biophysics*, vol. 395, pp. 41–48, 11 2001.

[76] D. L. Bader, D. M. Salter, and T. T. Chowdhury, "Biomechanical influence of cartilage homeostasis in health and disease," *Arthritis*, vol. 2011, pp. 1–16, 9 2011.

[77] E. Cambria, S. Brunner, S. Heusser, P. Fisch, W. Hitzl, S. J. Ferguson, and K. Wuertz-Kozak, "Cell-Laden Agarose-Collagen Composite Hydrogels for Mechanotransduction Studies," *Frontiers in Bioengineering and Biotechnology*, vol. 8, p. 346, 4 2020.

[78] "KEGG PATHWAY: Hippo signaling pathway - Homo sapiens (human)."

[79] Y. Deng, A. Wu, P. Li, G. Li, L. Qin, H. Song, and K. K. Mak, "Yap1 Regulates Multiple Steps of Chondrocyte Differentiation during Skeletal Development and Bone Repair," *Cell Reports*, vol. 14, pp. 2224–2237, 3 2016.

[80] S. Wang, L. Zhou, L. Ling, X. Meng, F. Chu, S. Zhang, and F. Zhou, "The Crosstalk Between Hippo-YAP Pathway and Innate Immunity," *Frontiers in Immunology*, vol. 11, p. 323, 2 2020.

Supplementary Material

S1 Additional Methods

Cell culture of HEK293 cells

HEK293 cells were cultured in T175 flasks in proliferation medium (DMEM with 10% FBS (fetal bovine serum), 100 Uml^{-1} penicillin and 100 gml^{-1} streptomycin). To passage the cells, they were washed with PBS (1x) and trypsinised using a trypsin-EDTA 0,25%/0.1 M solution and reseeded in a new flask at 1 million cells per 175 cm^2. Cells were used at passage 22-28 for the experiments.

Trizol method

Total RNA was obtained using TRIzol™ Reagent (Invitrogen) following the protocol described by the supplier. The RNA pellet was air dried for 5-10 minutes and resuspended in RNase-free water, followed by incubation at $55 - 60°C$ for 10-15 min. Samples were then frozen at $-80°C$ for further use.

Trizol disruption and column based extraction

Samples were lysed with TRIzol™ Reagent, mixed with 1 volume 70% ethanol and then transferred to the RNeasy MinElute spin column to proceed with the column extraction protocol as described in 3.9. Samples were then frozen at $-80°C$ for further use.

Agarase pre-treatment

Agarase(Thermo Fisher Scientific) was used to dissolve the agarose around the chondrocytes. For this, samples were first washed with PBS (1x) and heated to $70°C$ for 10 min and then cooled for 5 min at $42°C$. Agarase was added (0,2 U in HBE buffer) and incubated for 30-40 min. Samples were then frozen at $-80°C$ for further use.

Table (S1.0) Additional primers used for primer validation and housekeeping gene stability (B2M), 5' > 3', * indicates primers of own design

Gene	Forward	Reverse
B2M	GACTTGTCTTTCAGCAAGGA	ACAAAGTCACATGGTTCACA
CYR61 (CCN1) *	AGTGGGTCTGTGACGAGGAT	GGGTTTCTTTCACAAGGCGG
ARHGEF17 *	ACAAACCACCTCCTCCTGTG	GGTGTTCCATCAGGAATGCT
ARHGEF18 *	CAGGTGAAAATGGGGAGAGA	CTCCACCAGCACTGGGTATT
Col1A1	GTCACCCACCGACCAAGAAACC	AAGTCCAGGCTGTCCAGGGATG
ADAMTS5 S1	CCCACCCAATGGTAAATC	GACTCCTTTTGCATCAGAC
ADAMTS5 S2	TGATGGCCATGGTAACTG	GAATGTCAGGTTGCACTG
ADAMTS5 S3	TTTCTCCAAAGGTGACCG	AGTTCTCACACACTTCCC

S2 Additional Data

S2.1 Viability staining on chip

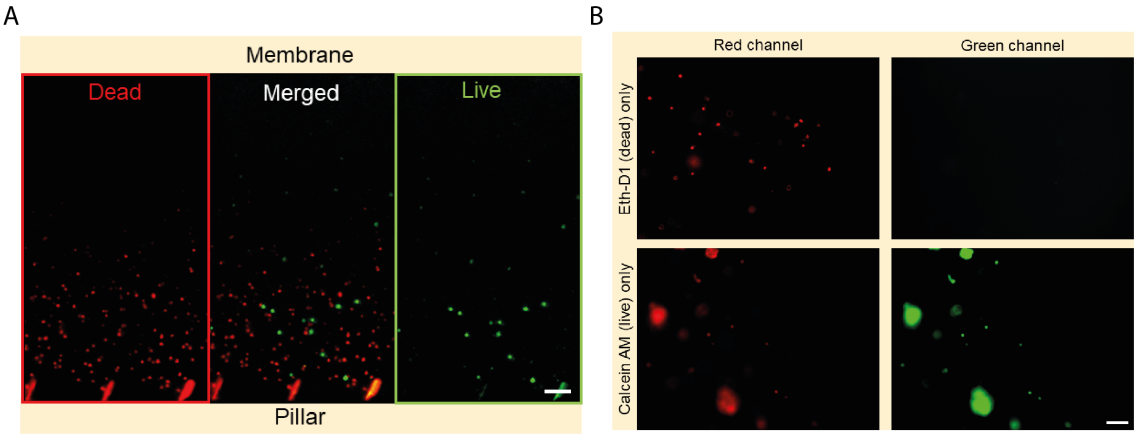

Figure (S2.1) Live/dead staining of HPC showing (A) Static chip with limited diffusion when the staining is injected into the medium channel. The hydrogel is therefore removed from the chip for homogeneous staining of the sample. (B) Static chip with either live or dead staining showing bleedthrough of the live staining into the red channel. Scalebar = 100 µm.

S2.2 Validation of RNA extraction methods

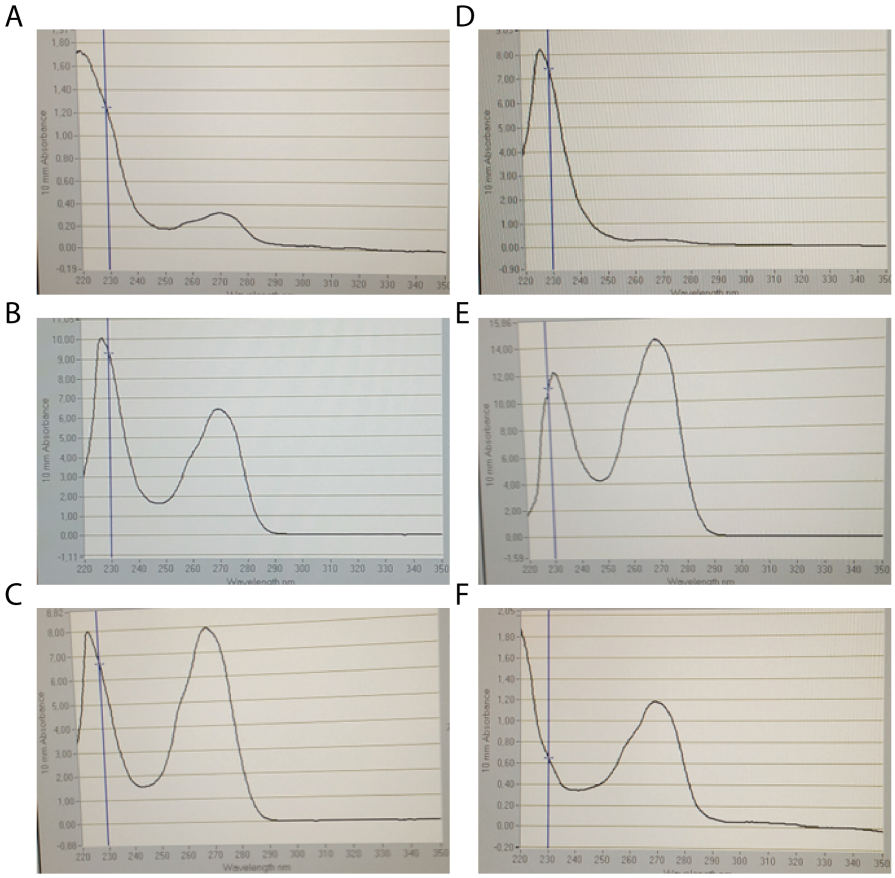

Figure (S2.2) Absorption spectra measured by Nanodrop of RNA samples extracted through (A) Column (RNeasy Microkit) (B) Trizol (phase separation) (C) Trizol+Column (D) No cell control Column extraction (E) Agarse+Trizol and (F) No cell control Trizol+Column extraction. All show high contamination at 230 nm, causing low 260/230 ratios. Extraction with Trizol shows high contamination at 270 nm with a wide peak, causing high readouts of RNA concentration. No cell control shows that the Column extraction has the least contamination at 260 nm.

S2.3 Primer validation

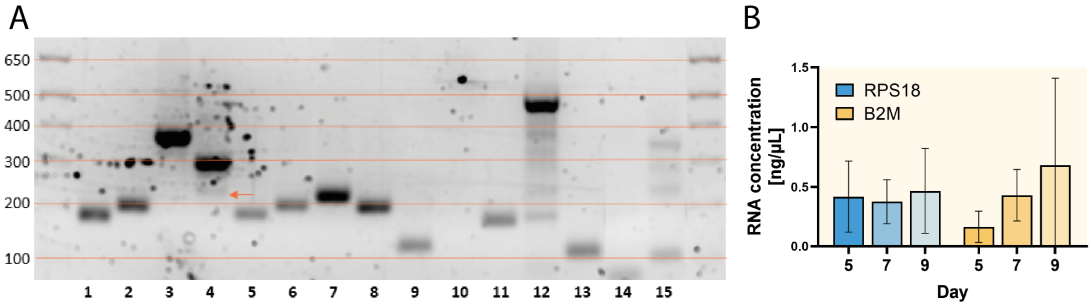

Figure (S2.3) Primer validation using a monolayer of HPC passage 4 cultured for 1 day (A) Gel electrophoresis of (1) RPS18 (180 bp), (2) YAP1 (203 bp),(3) CTGF- (385 bp),(4) CYR61 (315 bp),(5) ARHGEF17 (193 bp),(6) ARHGEF18 (218 bp),(7) ID-2 (237 bp),(8) Pai-1 (212 bp),(9) hAcan (136 bp),(10) Col10A1 (129 bp),(11) MMP13 (184 bp),(12) Col2A1 (92 bp),(13) Col1A1 (121 bp),(14) ADAMTS5 S1 (76 bp),(15) ADAMTS5 S2 (109 bp). First and last slot show a gene ladder, the scale indicated on the left, the orange arrow indicates a faint band under CYR61. Most primers show a band comparable to the size of the primer, with exception of Col2A1 which also shows several other bands. Col10A1 does not show any band, likely due to the short culture period and being a hypertrophy marker. ADAMTS5 S2 shows several products. (B) Stability of housekeeping genes RPS18 and B2M over time showing starting RNA concentration after RT-qPCR (N=3 chips), both show good performance ($R^2 = 0.998$), however RPS18 reveals a more stable concentration over time compared to B2M and will therefore be used as housekeeping gene.

Table (S2.3) Raw data CFX384 qPCR primer test, Baseline Threshold is determined by baseline between 3-10 cycles and the Threshold is taken at 2529,48 RFU. Samples are used in gel electrophoresis for primer validation.

Well	Sample	Cq	Melt Temp	Peak Height	Begin Temp	End Temp
A07	RPS18, 3	20.97	81.50	1361.23	77.00	87.00
B07	YAP, 3	26.23	82.50	1252.80	76.00	88.00
C07	CTGF-, 3	25.77	85.50	1375.69	80.50	95.00
D07	CYR61, 3	25.89	86.50	700.19	84.00	95.00
E07	ARHGEF17, 3	31.10	87.00	1156.78	77.50	95.00
F07	ARHGEF18, 3	29.29	81.50	1237.98	74.50	94.00
G07	ID2, 3	24.65	85.00	1414.41	80.50	94.00
H07	Pai-1, 3	26.59	84.50	1283.19	79.50	95.00
I07	Acan, 3	26.76	84.00	854.38	79.50	95.00
J07	Col10A1, 3	39.08	None	None	None	None
K07	ADAMTS4, 3		None	None	None	None
L07	MMP13, 3	29.61	78.00	1178.02	74.50	84.50
M07	COL2A1_NG, 3	31.36	89.00	591.31	78.50	92.50
N07	COL2A1_HAY2, 3	26.32	89.50	713.38	81.50	95.00
O07	COL1A1, 3	23.40	87.50	733.12	81.00	94.00

Table (S2.3) Primer efficiency and amplification factor calculated from serial dilutions, only the primers that will be used later are shown.

Target	Slope	Efficiency	R^2	Amplification
RPS18	-3.621	88.87%	0.9993	1.889
YAP	-3.156	107.42%	0.9710	2.074
CTGF	-3.923	79.84%	0.9980	1.798
Pai-1	-3.518	92.42%	0.999	1.924
Id2	-3.513	92.60%	0.9958	1.926
hAcan	-2.743	131.50%	0.9408	2.315
MMP13	-3.102	110.07%	0.9862	2.101

S2.4 Immunofluorescence monolayer antibody validation

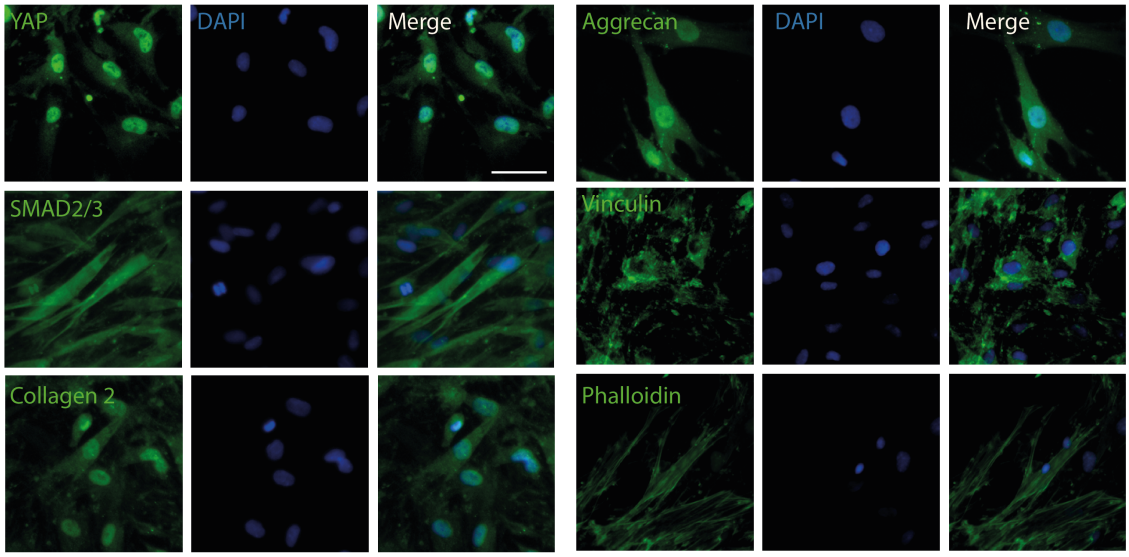

Figure (S2.4) Immunofluorescence images of HPC monolayer at day 14 validating several ABs. Dilutions used are YAP (1:50), SMAD2/3 (1:600), Col2a1 (1:100), Acan (1:100), Vinculin (1:50), Phalloidin (1:200), AF288 (1:200) and AF647 (1:200). SMAD1/5/9 AB is not shown because the image quality was poor, but did show staining in ohter samples. Scalebar = 50 µm.

S2.5 Immunofluorescence on chip controls

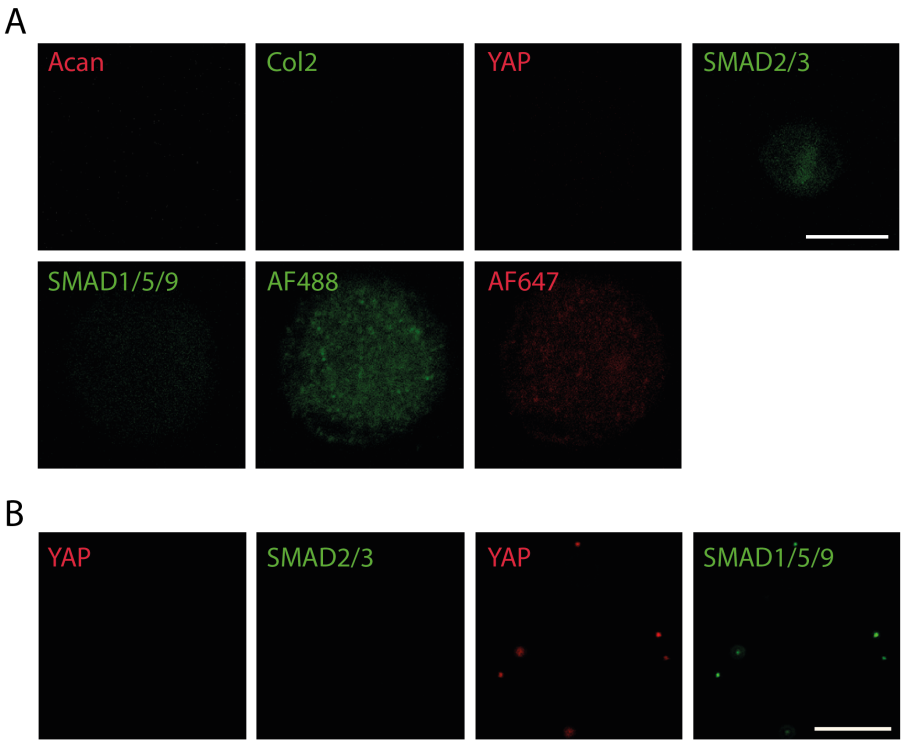

Figure (S2.5) Immunofluorescence control images of HPC in static chip at day 12 (A) Primary or secondary AB only control showing some autofluorescence of SMAD2/3 and AF488. Brightness is adjusted slightly to make this visible, therefore it is not expected to affect the analysis methods used to measure N/C ratio. (B) No cell control of agarose hydrogel mixed with medium using both primary and secondary ABs. The left images show no signal while the right images do show some signal in both channels, indicating signal from a-specific binding can be present in some chips. Scalebar = 10 µm.

S2.6 Viability of monolayer culture upon addition of cytokines

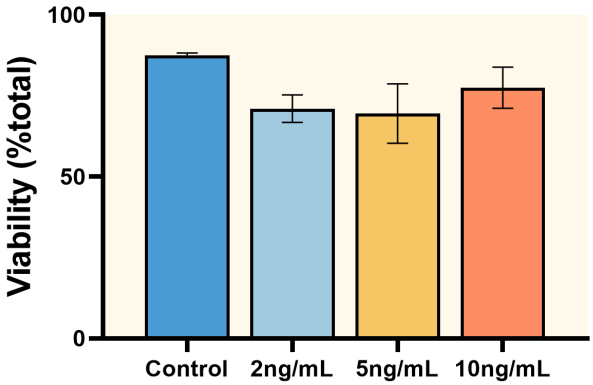

Figure (S2.6) Viability of HPC p4 in monolayer culture (25000 cells/cm^2) after addition of 2, 5 or 10 ng/mL of cytokines IL-1β and TNF-α (N=2 wells). The addition of cytokines shows a slight decrease in viability, however no downward trend is observed with increasing cytokine concentration. The data suggests that all applied concentrations do not significantly decrease the viability of chondrocytes.

S2.7 Chip seeding quality

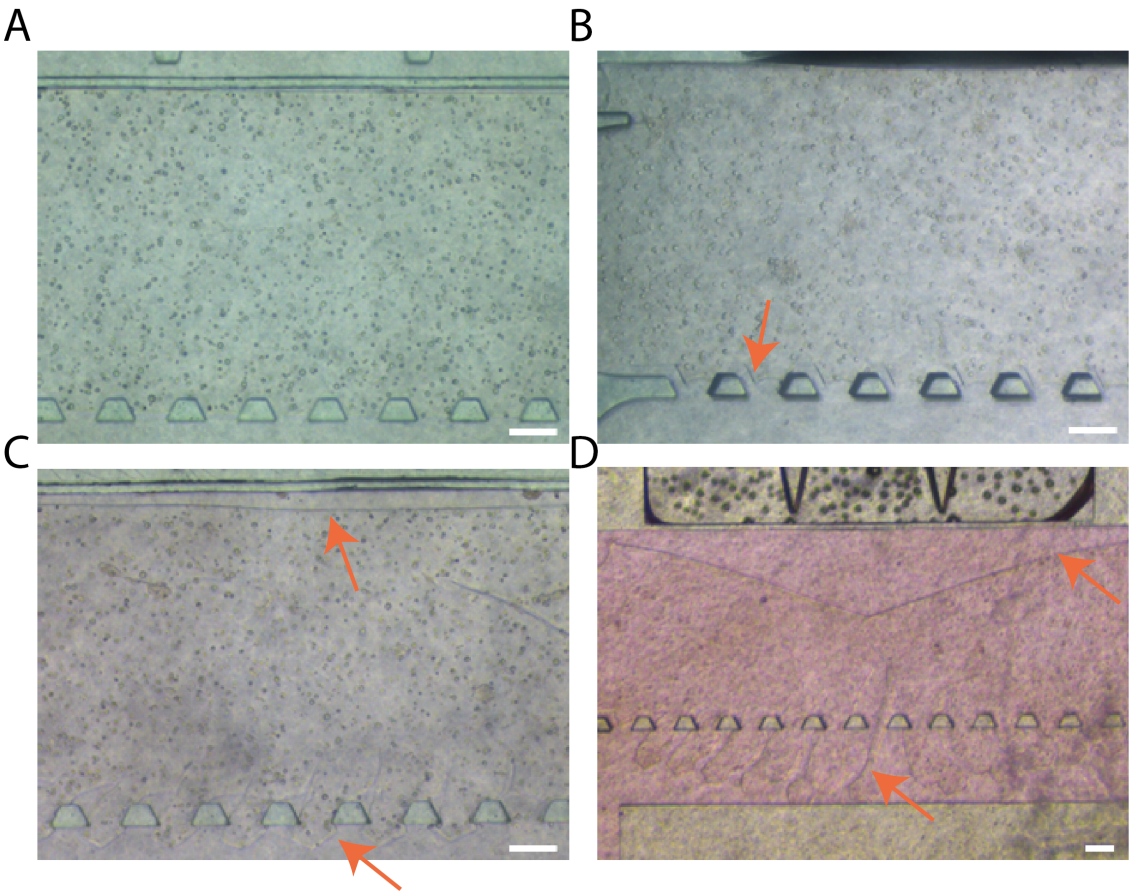

Figure (S2.7) Chips after agarose-cell seeding showing different conditions of quality: (A) Good quality chip, no gap is shown between the garose and membrane or pillars. (B) A small gap is indicated by the arrow, which causes the gel to move within the chip during actuation. (C) and (D) show a chip after compression, the bottom arrow shows where the agarose has broken through the pillars and the top arrow indicates the gap between the agarose and membrane. (D) is not used for analysis while (C) could be used depending on the analysis, scalebar = 100 µm.

S2.8 Influence of pressure magnitude on protein nuclearisation

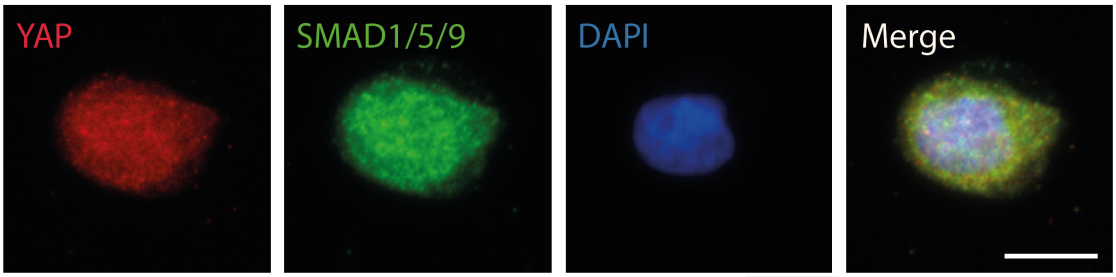

Figure (S2.8) Influence of a single dynamic compression session with 300 mbar at day 5 of HPC. Immunofluorescence images of single cells representative for YAP and SMAD2/3, both have a N/C ratio around 1.3, scale bar = 10 µm.

S2.9 Statistical analysis of dynamic compression over time

Table (S2.9) Statistical analysis of dynamic compression over time, complement to Figure 5.1B, Pvalues: $0.001 < P <= 0.01^{**}$, $0.0001 < P <= 0.001^{***}$, $P <= 0.0001^{****}$

	YAP	SMAD2/3	SMAD1/5/9
Static D5 vs. Static D9	ns	**	ns
Static D5 vs. Static D12	****	****	ns
Static D5 vs. 300 mbar D5	ns	**	ns
Static D9 vs. Static D12	****	****	ns
Static D9 vs. 300 mbar D9	ns	****	ns
Static D12 vs. 300 mbar D12	ns	ns	ns
300 mbar D5 vs. 300 mbar D9	***	****	ns
300 mbar D5 vs. 300 mbar D12	****	****	****
300 mbar D9 vs. 300 mbar D12	****	ns	ns

S2.10 Validation of TGF-β1 ELISA on chip samples

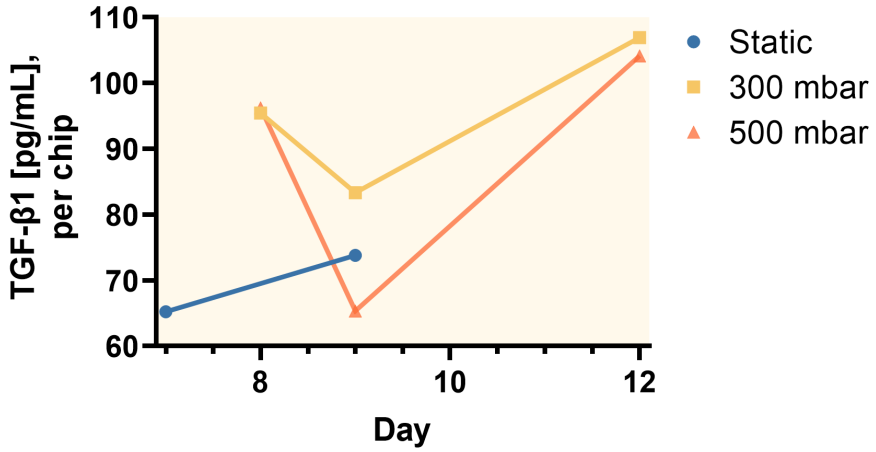

Figure (S2.10) TGF-β1 ELISA validation comparing static, 300 mbar and 500 mbar compression conditions. TGF-β1 concentration per chip indicating it is possible to detect TGF-β1 from pooled samples (sensitivity of >8 pg/mL). However, many data points are excluded as they did not pass the threshold value of the no cell control, thus the dilution of samples should be reduced. Note that the data is not normalised to DNA quantity, the conditions are however from the same experiment. N=2 medium samples of 6 chips pooled

S2.11 TGF-β1 concentration over time in normal and pathological conditions

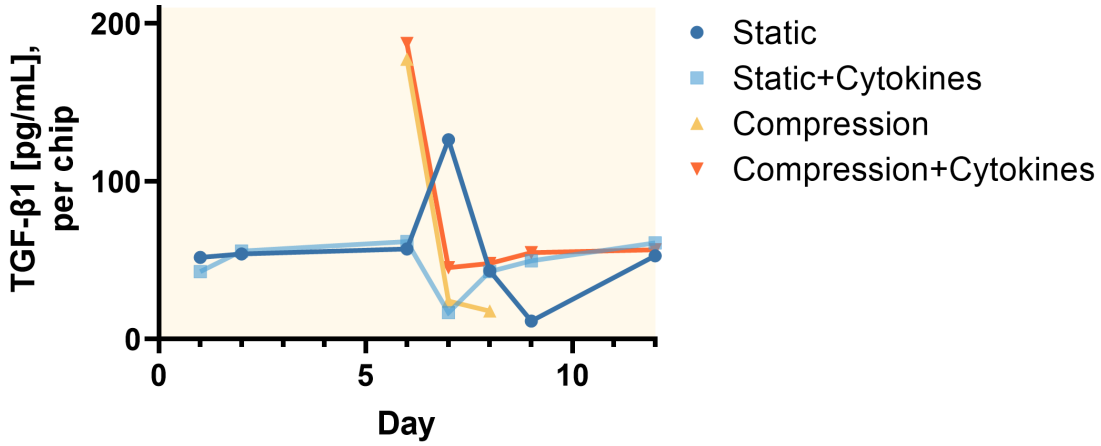

Figure (S2.11) TGF-β1 concentration from ELISA normalised to DNA quantity, comparing normal and pathological conditions. Both static conditions start and end with a concentration around 51 pg/µL. The concentration in mechanically stimulated conditions is initially increased after 1 day of stimulation, which decreases again toward this 51 pg/µL.

S2.12 Viability in normal and pathological conditions on chip

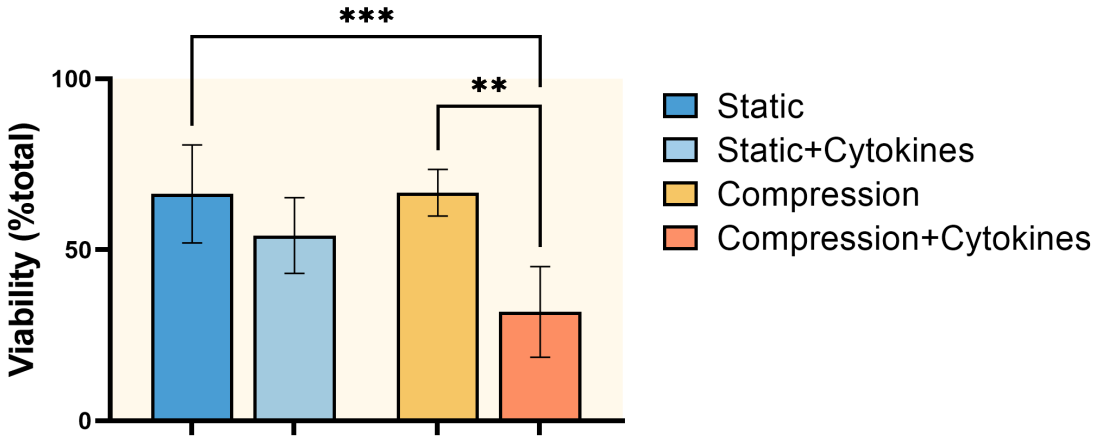

Figure (S2.12) Viability of HPC on chip in static and compressed (300 mbar) conditions with and without the addition of cytokines, day 12. While cytokines in static condition do not significant difference, in combination with compression there is a significant difference. The cells were visually inspected throughout the experiment and cells looked viable. This significant difference might be due to the analysis method and only one replicate used. N=1, Pvalues: $0.001 < P <= 0.01^{**}$, $0.0001 < P <= 0.001^{***}$

S3 ImageJ Macro for viability cell counting

```
//generalization
titleOrig = getTitle();

run("Split Channels");
//selectWindow(titleOrig + " (blue)");

//Dead
selectWindow(titleOrig + " (red)");
//run("Enhance Contrast", "saturated=0.35");
//run("Apply LUT");
setMinAndMax(0, 50);
run("Gaussian Blur...", "sigma=1");
run("Subtract Background...", "rolling=5 create");
setAutoThreshold("Triangle dark");
setOption("BlackBackground", true);
run("Convert to Mask");
run("Analyze Particles...", "size=50-Infinity circularity=0.60-1.00 display exclude clear add");

waitForUser

//Live
selectWindow(titleOrig + " (green)");
//run("Enhance Contrast", "saturated=0.35");
//run("Apply LUT");
run("Subtract Background...", "rolling=5 create");
setAutoThreshold("Triangle dark");
run("Convert to Mask");
run("Analyze Particles...", "size=50-Infinity circularity=0.60-1.00 display exclude clear add");

waitForUser


//Both
imageCalculator("AND create", titleOrig + " (red)",titleOrig + " (green)");
selectWindow("Result of " + titleOrig + " (red)");
run("Analyze Particles...", "size=5-Infinity circularity=0.20-1.00 display exclude clear add");

waitForUser
close("*")
```